1-1-2013

Vapor-Liquid-Solid Growth of Semiconductor SiC Nanowires for Electronics applications

Rooban Venkatesh K G Thirumalai

Vapor-liquid-solid growth of semiconductor SiC nanowires for electronics applications

By

Rooban Venkatesh Kulandaivelu Govindarajulu Thirumalai

A Dissertation
Submitted to the Faculty of
Mississippi State University
in Partial Fulfillment of the Requirements
for the Degree of Doctor of Philosophy
in Electrical Engineering
in the Department of Electrical and Computer Engineering

Mississippi State, Mississippi

August 2013

Vapor-liquid-solid growth of semiconductor SiC nanowires for electronics applications

By

Rooban Venkatesh Kulandaivelu Govindarajulu Thirumalai

Approved:

Yaroslav Koshka Professor Electrical and Computer Engineering (Major Professor)	Raymond S. Winton Professor Electrical and Computer Engineering (Committee Member)
Albert Davydov Project Leader National Institute of Standards (Committee Member)	Erdem Topsakal Associate Professor Electrical and Computer Engineering (Committee Member)
Robert B. Reese Associate Professor Electrical and Computer Engineering (Committee Member)	James E. Fowler Professor Electrical and Computer Engineering (Graduate Coordinator)

Royce O. Bowden
Interim Dean of the Bagley College of Engineering

Name: Rooban Venkatesh Kulandaivelu Govindarajulu Thirumalai

Date of Degree: August 17, 2013

Institution: Mississippi State University

Major Field: Electrical Engineering

Major Professor: Dr. Yaroslav Koshka

Title of Study: Vapor-liquid-solid growth of semiconductor SiC nanowires for electronics applications

Pages in Study: 95

Candidate for Degree of Doctor of Philosophy

While investigations of semiconductor nanowires (NWs) has a long history, a significant progress is yet to be made in silicon carbide (SiC) NW technologies before they are ready to be utilized in electronic applications.

In this dissertation work, SiC NW polytype control, NW axis orientation with respect to the growth substrate and other issues of potential technological importance are investigated. A new method for growing SiC NWs by vapor-liquid-solid mechanism was developed. The method is based on an in-situ vapor phase delivery of a metal catalyst to the growth surface during chemical vapor deposition. This approach is an alternative to the existing seeded catalyst method based on ex-situ catalyst deposition on the target substrate.

The new SiC NW growth method provided an improved control of the NW density. It was established that the NW density is influenced by the distance from the catalyst source to the substrate and is affected by both the gas flow rate and the catalyst diffusion in the gas phase. An important convenience of the new method is that it yields NW growth on the horizontal substrate surfaces as well as on titled and vertical sidewalls

of 4H-SiC mesas. This feature facilitates investigation of the NW growth trends on SiC substrate surfaces having different crystallographic orientations simultaneously, which is very promising for future NW device applications.

It was established that only certain orientations of the NW axes were allowed when growing on a SiC substrate. The allowed orientations of NWs of a particular polytype were determined by the crystallographic orientation of the substrate. This substrate-dependent (i.e., epitaxial) growth resulted in growth of 3C-SiC NWs in total six allowed crystallographic orientations with respect to the 4H-SiC substrate. This NW axis alignment offers an opportunity to achieve a limited number of NW axis directions depending on the surface orientation of the substrate. The ease of controlling the NW density enabled by the vapor-phase catalyst delivery approach developed in this work, combined with the newly obtained knowledge about how to grow unidirectional (well-aligned) NW arrays, offer new opportunities for developing novel SiC NW electronic and photonic devices.

DEDICATION

I dedicate this work to my dear parents and my loving wife.

ACKNOWLEDGEMENTS

This work was only made possible by my advisor Dr Yaroslav Koshka; he has been my mentor and has helped me throughout my Ph.D. He has been very supportive from the beginning and has helped me through some difficult choices. I would like to sincerely thank him for his encouragement, guidance and all the trust he put in me.

I would also like to thank our collaborators at NIST for their help with characterization through the entire duration of the project, especially Dr Davydov from NIST for his ideas, expertise with semiconductor NWs and expertise in crystallographic characterization. I would also like to thank Dr Neil Merrett (AFRL) for his invaluable help with designing electrical test structures, semiconductor device fabrication and many other things. I would also like to thank my committee members Dr. Reese, Dr Topsakal and Dr Winton for their value inputs for my dissertation.

I would also like to thank my colleagues Dr. Bharat Krishnan, Dr. Siva Kotamraju and Dr Hrishkesh Das for their support, guidance and friendship. In addition I would to offer special thanks to the I^2AT center staff Richard Kuklinski, Bill Monroe and Amanda Lawrence for training me to proficiently use TEM, SEM, XRD and EDS used in this work.

TABLE OF CONTENTS

LIST OF FIGURES

KEYWORDS & DEFINITIONS

Substrate: A small thin section of single crystal semiconductor material which in our case our 4H-silicon carbide.

Chemical Vapor Deposition (CVD): A chemical process commonly used to grow high purity epitaxial layer on top of substrate.

Epitaxy: A process of depositing material on a substrate such that the deposited layer replicates the structure of the underlying layers. The layer or deposited material is called as epitaxial layer. Stacking Faults: It is a type of planar defect caused by interruption of the stacking sequence. It is quite common among close packed structures like Hexagonal Close packed and Face centered Cubic structures.

Basal plane: The plane perpendicular to the axis of the crystal.

Stagnant Layer: The region in the gas phase located right above the substrate surface where the gas flow velocity is assumed to be zero.

CMOS: complementary metal oxide semiconductor.

Debye screening length: A term used to define the region in which mobile charge carriers screen out external electrical field.

Hot zone: A hot region at the center of a CVD reactor where precursor gas dissociation takes place upon entry.

C/Si ratio: The ratio between carbon to silicon molecules provided by the growth precursors.

Light emitting Diode (LED): Semiconductor devices capable of emitting light during the flow of the electric current.

Laser: An acronym for "Light Amplification by Stimulated Emission of Radiation". A device capable of producing spatially coherent light with low dispersion.

CHAPTER I

INTRODUCTION

1.1 History of nanotechnology

The term nanotechnology was coined and first used by Dr. Norio Taniguchi, a professor at Tokyo University of Science in his paper "On the Basic Concept of Nano-Technology" in 1974[1]. He used this term to describe semiconductor processes such as ion beam milling that were advancing to a point where processing of materials at a molecular or atomic scale was realizable. Though the term was introduced only in 1974, its concepts were seeded much earlier by Richard Feynman. Feynman was a theoretical physicist who received the Nobel Prize in Physics in 1965 for his contribution to quantum electrodynamics, but he is also was well known for his introductory lectures on Physics named "The Feynman Lectures on Physics". He introduced the concept of nanotechnology on his talk entitled "There is plenty of room at the bottom" [2]. He considered interesting possibilities associated with the ability to manipulate matter on an atomic scale. He envisioned the bottom-up approach of fabrication, which would allow arranging atoms in any order as we see fit. He was particularly interested in the possibility of higher-density circuitry, high density storage and more importantly the need for high resolution microscopes. His vision was later realized starting with the invention of scanning tunneling microscope (STM) in 1981, which accelerated the progress in

nanotechnology. His concept inspired many others physicists including Eric Drexler who brought awareness of nanotechnology among public.

The importance of nanotechnology grows so fast that in the year 2000 a federal nanoscale science, engineering and technology research program known as National Nanotechnology Initiative (NNI) was implemented. This initiative is outlined in "http://www.nano.gov/goaloneobjectives" as follows:

1. "Advance a world-class nanotechnology research and development (R&D) program;
2. Foster the transfer of new technologies into products for commercial and public benefit;
3. Develop and sustain educational resources, a skilled workforce, and the supporting infrastructure and tools to advance nanotechnology; and
4. Support responsible development of nanotechnology."

In the year 2003, a legislation known as 21st Century Nanotechnology Research and Development Act was passed authorizing expenditure up to $3.63 billion for five of the 25 NNI participating agencies. The cumulative investment under NNI since its inception is $18 billion. These funding opportunities spurred steady growth in nanotechnology research and investment. It has also enabled continuous growth of nanotechnology or nanoscience community. The details of NNI, publications from its funds, etc are available online at "www.nano.gov".

It is very crucial to recognize the reason for this drastic growth of nanotechnology-related research and investments. The main reason for the excitement about nanotechnologies is their applications. Although the ability to manipulate mater on

the atomic scale was first envisioned along the lines of making smaller and faster circuitry, the applications of such high precision engineering are infinite. Despite these continuous advances, many areas of nanoscience require extensive investigation and development before the full potential of nanotechnologies can be realized.

1.2 Semiconductor nanostructures and their applications

The main goal of nanotechnologies is the fabrication and application of nanostructures. Nanostructures have many interesting properties owing to their dimensions such as quantum confinement, ballistic transport, high young's modulus etc. These interesting properties can benefit many applications such as high performance circuits, chemical and biological sensors, photonic devices (e.g., lasers and LED), etc[3].

1.2.1 Classification of nanostructures

Nanostructures can be classified into three categories based on the number of dimension which are in the nanometer range. 0-D nanostructures are structures in which all the three dimensions are in nanometer scale. A popular example is a nanoparticle, which can be also called a quantum dot. 1-D nanostructures are structures in which two dimensions are in nanometer scale (e.g., a nanowire). 2-D nanostructures are those structures which have only one dimension in nanometer scale (e.g., graphene). It is important to note that quantum effects occur only when the dimension of the nanostructure is comparable to its electron wavelength, and they are more pronounced as the size of nanostructure is reduced. Properties of nanostructures

Nanostructures owe their unique properties to two main reasons. The first reason is their very small size; since at least one of the dimensions is in the nanometer range,

they show quantum effects. The second reason is that since nanostructures have high surface to volume ratio, they have higher surface free energy compared to bulk material. These two properties (along with many others not mentioned here) give rise to interesting applications.

Let us discus quantum confinement effects. An electron in a bulk material act similar to a free particle since the equivalent wavelength of an electron is much smaller than the dimensions of the confining bulk material. However, the situation changes as the dimensions of the material are reduced down to a critical dimension that is close to the wavelength of the electron. When such dimensions are reached, the spectrum of the allowed energy values of the electron becomes discrete, and it also causes widening of the semiconductor bandgap, which is often observed as a so called blue shift of the light, where the wavelength of light emitted decreases and shifts towards the higher-energy blue region. This property can be used in blue LEDs or lasers based on quantum dots [4]. More in-depth consideration of the involved mechanisms reveals that the density of states in the conduction and valance bands also varies based on the number of dimensions that are confined. (Figure 1.1)

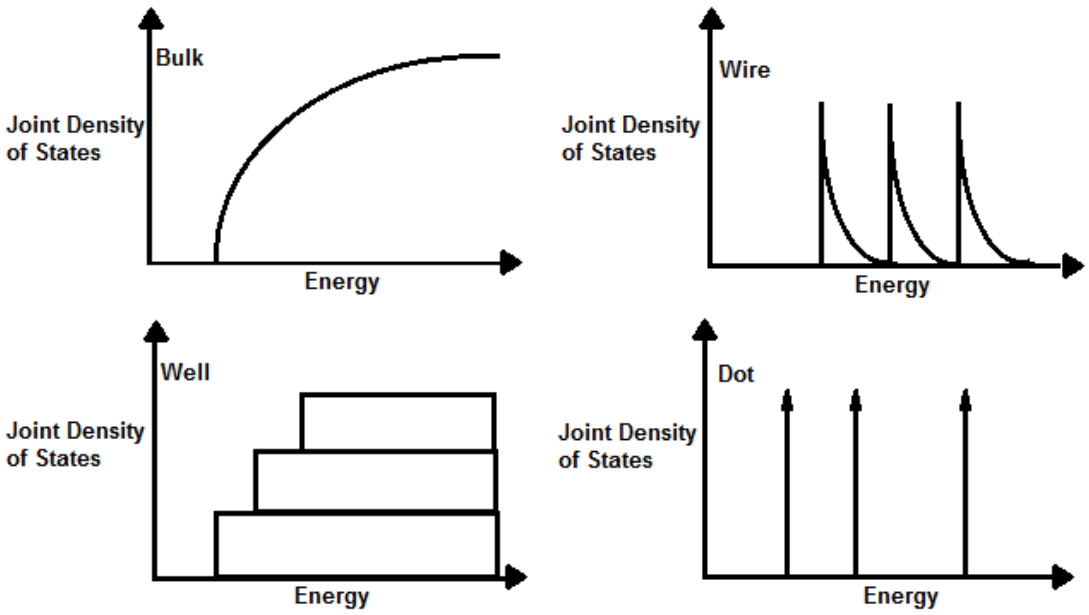

Figure 1.1 Comparison of the joint density of states in the conduction and valence band in a bulk semiconductor material and in nanostructures [5]

The second important effect is the high surface to volume ratio causing high surface free energy for a given volume in the case of nanostructures. High surface energy causes changes in the chemical and physical properties of materials such as the crystal structure, Young's modulus, melting point, etc [6]. This high surface energy can be beneficial for application of nanostructures in catalysis[7]. In addition to causing high free surface energy, a relatively large surface of an otherwise tiny semiconductor structure/device is very beneficial by itself. The large surface-to-volume ratio of nanowires is taken advantage of in sensor applications [8–10] to achieve higher sensitivity.

1.3 SiC Nanowires, their promising applications and their problems

As discussed in the previous section, nanostructures have properties which can be used in many interesting applications. Many applications require very specific nanostructures made of a material with certain physical properties. The need for SiC NWs is justified in this section, along with a discussion of the most promising applications of SiC NWs.

1.3.1 Need for novel semiconductor materials and devices

Moore's Law predicts an approximate doubling of the transistor count on an integrated circuit (IC) every two years[11]. Technologists in semiconductor industry have worked hard to continue compliance with this law by introducing continuous as well as disruptive improvements and advances in IC fabrication technologies.

The 2010 International Technology Roadmap for Semiconductors (ITRS) predicts slowing down of the trend of exponential growth in computing power at the end of 2013[12]. This slowdown in improving the density of transistors is attributed to several problems associated with scaling. Scaling is a process of reducing feature size of the transistor in order to increase its speed and transistor density. This scaling, which has been the driving force for Moore's law, brings drawbacks such as high leakage current in transistors, inability of Si to efficiently dissipate the increased heat, growing fabrication costs associated with extreme ultraviolet lithography (EUVL) and other lithographic techniques needed for further scaling, etc.

These problems of scaling the traditional complementary metal-oxide-semiconductor (CMOS) technology forced scientists and engineers to look for alternative processes, device designs, and methodologies. Some of possible alternatives to the

conventional active devices and interconnects are NWs and carbon nanotubes (CNTs)[13]. Their superior electrical and thermal properties and their small dimension can provide much higher device density.

Many different implementations of NW-based devices are currently under investigation, e.g., the use of semiconductor NW heterostructures [14], the use of completely different from CMOS device physics such as a single electron transistor (SET)[15], and many others. Regardless of their implementation, NWs are considered to be very promising for large-scale integrated circuits [14], [15].

NW sensors represent another very promising area of research. NWs have a large surface to volume ratio, which makes them a perfect candidate for ultrasensitive sensors. Their small diameters comparable to the Debye screening length ensure significant changes in electrical properties in response to minor perturbations. In some applications such as chemical detection [16] and bio-sensors [17], the key requirement is high sensitivity which can be drastically enhanced by using sensing elements made of NWs. In addition, temperature sensors, pressure sensors, flow sensors, etc using a NW as a sensing element [9], [10], [18] can provide better response time compared to sensors that use conventional FETs. Another advantage of NW-based sensors is the reduced threshold power densities resulting in lower power consumption compared to conventional sensors [19].

The range of applications of NW-based devices and their commercial potential can significantly expand as more durable and versatile materials are employed. One such material, which has many unique properties, is silicon carbide (SiC), which is the focus of this study.

1.3.2 SiC NW devices and their problems

Silicon carbide (SiC) is a wide band gap semiconductor that is being aggressively developed for high power and high temperature applications because of its high electrical breakdown strength and high thermal conductivity [20][21][22]. Silicon carbide also has high Young's modulus, good chemical inertness and high radiation hardness[19] [22]. These properties make it an excellent candidate for the fabrication of nanodevices capable of operating in harsh environments. Some of the most promising applications of SiC-based nanodevices are discussed below.

1.3.2.1 SiC Nanowire Field Effect Transistor

One of the main applications of SiC NWs is their use in nanowire field-effect transistors (NWFETs). NWFET's principle of operation is similar to that of conventional metal oxide semiconductor field effect transistor (MOSFET). In conventional MOSFETs a bias potential is applied to the gate, which effectively controls the semiconducting channel underneath. However, in the case of NWFET, instead of the inversion region of MOSFET or the non-depleted portion of the channel in JFET, the entire cross-section of the NW may serve as the channel. Figure 1.2 presents a few common implementations of NWFETs.

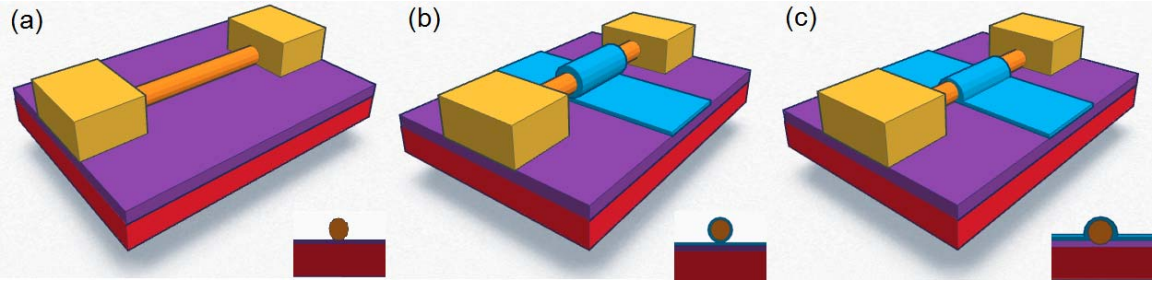

Figure 1.2 Different configurations of NWFET gating. Insets showing their respective cross section: (a) Back gate, (b) semi cylindrical top gate, and (c) cylindrical gate. [24]

There are several potential advantages of NWFETs in general compared to conventional FETs such as very small feature size below the limit of conventional lithography, less pronounced effects of scaling on device characteristics and lower carrier scattering when radial or axial NW heterostructures are employed[25][26] [24]. Use of SiC NWs in NWFETs add to these advantages by providing benefits such as high temperature and high power operation [27]. There have been many attempt recently to fabricate SiC NWFET, which provided some insight into electrical and optical properties and the main areas of improvement [27–31]. These attempts showed SiC NWFET's strong potential for resolving many of the scaling issues of conventional FETs, but they still have a number of problems, which need to be addressed before SiC NWFETs can be commercially viable. A NW growth process that can be integrated into current IC fabrication processes without much change to avoid significant increase of the fabrication costs has to be developed. Better control of the SiC NW density, polytype, and growth orientation is to be achieved. Metal contact formation to NWs needs to be further improved since experimentally achieving ohmic contacts is difficult. Use of silicide

contacts has yielded much better results, but more progress in this direction is crucial for further development of SiC NWFET.

1.3.2.2 SiC Nanosensors

SiC NWs provide high chemical stability and biocompatibility which makes them very promising for biomedical applications[32] [33][34][35]. In recent studies SiC was found to be biocompatible, which allows it to be used for minimally invasive sensors/probes for tissue monitoring during organ transplant[36]. In addition these studies concluded that SiC probes outperforms Si probes with four fold higher tolerance to crack or rupture and also it showed a tenfold higher operating bandwidth in comparison to Si based probes.

As discussed above, scaling is a common practice in semiconductor industry aimed at increasing the device density and the operating frequency, but as the dimensions decrease, it makes the electrical conductance of the device more sensitive to analyte adsorption at the device surface [16]. This property is taken advantage of by NW-based devices and is used to achieve improved sensor sensitivity. By functionalizing the SiC NW with different receptors, various analytes can be detected [37][36]. Also, NWFETs utilizing SiC NWs are more durable and capable of handling harsh environments thanks to the physical properties of SiC[27].

There are many areas where SiC NWs need improvement to be ready for commercial sensor applications, especially the control of the NW alignment, orientation and polytype.

1.4 The scope and organization of this dissertation

This dissertation is primary focused on addressing certain issues that prevent SiC NWs from realizing their full potential. It develops an alternative catalyst delivery mechanism to address the limitations of current NW growth methods such as good SiC NW density and crystalline quality. It also suggests how the current method has been used to achieve low density NWs for investigation of NW properties and explains the polytype and orientation dependence on substrate of the grown NWs. The characterization techniques used in this work to explain this new catalyst delivery method include X-ray diffraction, energy dispersive spectroscopy (EDS), transmission electron microscopy (TEM) and Electron Back Scatter Diffraction (EBSD)

This work is organized as follows

Chapter 1 gives an overview of the history of nanotechnology and its importance. It also discusses some of the interesting properties and applications of nanostructures especially those relevant to the silicon carbide nanowires (SiC NWs) and justifies the need for SiC NWs and their applications.

Chapter 2 provides the current state of knowledge related to NW synthesis methods relevant to SiC NW fabrication. It also briefly discusses pros and cons of each process and explains the reason behind the choice of synthesis method. Finally, it explains the theory and mechanism behind the chosen growth method in details.

Chapter 3 outlines the experimental arrangements such as the CVD setup and process parameters used our work. It also discusses sample preparation and outlines the different types of samples used it this work. It also gives an overview of metal contact

fabrication methods for electrical characterization and presents all the characterization methods used in this work.

Chapter 4 outlines of the results of the previous work on SiC NW growth in our group and describes how the NW growth process was further developed and modified to suit the objectives of this dissertation work. It explains in details the development of a new catalyst delivery method for SiC NWs. It further explains the dependence of this new catalyst delivery mechanism on parameters like C/Si ratio, metal catalyst proximity etc. It also outlines the features and benefits of this new method, investigates the orientation and polytype of the grown NW using all the characterization techniques describe in chapter 3 (XRD, EDS, EBSD, SEM,SAED etc) and suggest ways of obtaining well aligned NWs. It finally describes the initial attempts of measuring the electrical properties of the grown NW using two different methods.

Chapter 5 briefly summarizes all the results of this work and provides recommendations for the future studies.

CHAPTER II

CURRENT STATE OF KNOWLEDGE

2.1 Nanowire synthesis methods

Nanowire synthesis methods can be broadly classified into two categories: “top-down” and “bottom-up” approaches. Both these approaches are suited for NW synthesis, but certain NW synthesis methods are preferred over others depending on the applications and their requirements such as cost, polytype controllability, orientation, alignment etc. Some of the common methods of NW synthesis are discussed in detail in the forthcoming sections.

2.1.1 Conventional top-down approach

The top–down approach is the conventional method used in the semiconductor industry; it involves taking a large piece of starting material and selectively removing the unwanted regions by various patterning and etching techniques until the final desired feature is obtained. Since the inception of integrated circuits in 1950s, semiconductor industry followed this approach, which has given researchers ample time to significantly advance the approach and access its limitations. Photolithography, electron beam lithography, ion beam lithography, and nano-imprint lithography are some of the well-known fabrication methods that follow the top-down approach.

2.1.1.1 Lithography Techniques

The most common and conventional technique used to define a desirable pattern is photolithography. The minimum feature size possible with this technique is a function of the wavelength of the light used to expose the photoresist. This relation between the minimum feature size and the wavelength of the light source is exploited to achieve smaller feature size. The mercury vapor lamp (~400 nm wavelength) initially used in photolithography was later replaced by deep ultraviolet excimer lasers such as the Krypton fluoride laser (248-nm wavelength) and the argon fluoride laser (193-nm wavelength), which has brought the feature sizes down to 50nm [38]. Further reduction in the feature size is made possible by using other lithography techniques such as electron beam lithography, deep ultraviolet lithography and X-ray lithography.

E-beam lithography is one of newer methods capable of reducing feature size beyond conventional photolithography. In e-beam lithography, the pattern is drawn directly on a resist-covered sample. The main advantage of this method is its higher resolution, and the main disadvantage is its low throughput because it takes long time to expose a complete wafer.

The e-beam based top-down technique is relatively popular for NW fabrication. For example Si NWs with diameter of 80 nm formed by e-beam lithography followed by inductively coupled plasma (ICP) etching was reported in Ref. [39]. Some preliminary efforts to use the top-down approach for SiC NWs (or nanopillars) are reported in Ref.[40]. It was accomplished by first drawing circular Ni/Al/Cu mask with the diameter of 370nm on 4H-SiC substrate followed by SF_6/O_2 plasma etching resulting in 7μm long pillars.

2.1.2 Bottom-up approach for synthesis of NWs and other 1D nanostructures

The bottom-up approach involves arranging smaller components (e.g., molecules) into more complex assemblies (e.g., NWs). Most of the modern methods for NW synthesis use the bottom-up approach because of various reasons, which will be discussed in the forthcoming sections. Some of the more common methods used for the bottom-up SiC NW synthesis are briefly discussed below.

2.1.2.1 Synthesis of SiC nanowires from carbon nanotubes

In this method carbon nanotubes (CNTs) are allowed to react with SiO under a flow of Argon at 1700°C to form SiC whiskers [41][42]. This process resulted in SiC NWs with the length and diameter larger than the used CNTs. The chemical reaction of this process is as follows[42]:

$$2CNT(s) + SiO(g) \rightarrow SiC(s) + CO(g) \quad (2.1)$$

This technique also works with SiI_2 as reactant instead of SiO [43]. Ref.[44] describes a two-step process capable of synthesizing SiC nanorods from CNT at a much lower temperature of 1400°C. This two-step process involves

(1)Reaction between Silica (SiO_2) and Silicon (Si) to form SiO vapor (Eq.2.2)[42]

$$SiO_2(s) + Si(s) \rightarrow 2SiO(v) \quad (2.2)$$

(2) Reaction of SiO vapors with CNTs to form SiC nanorods (Eq. 2.3) [42].

$$SiO(v) + 2C(s) \rightarrow SiC(s) + CO(v) \quad (2.3)$$

In addition, CO_2 vapor from Eq. 2.4 could react with CNT to form CO[42].

$$C(s) + CO_2(v) \rightarrow 2CO(v) \quad (2.5)$$

When this reaction shown in E.q. 2.5 dominates, CNTs becomes thin and the SiC nanorods formed from these thin CNTs are much thinner than the initial CNT.

The method has not gained much popularity because of its high cost and low efficiency[42].

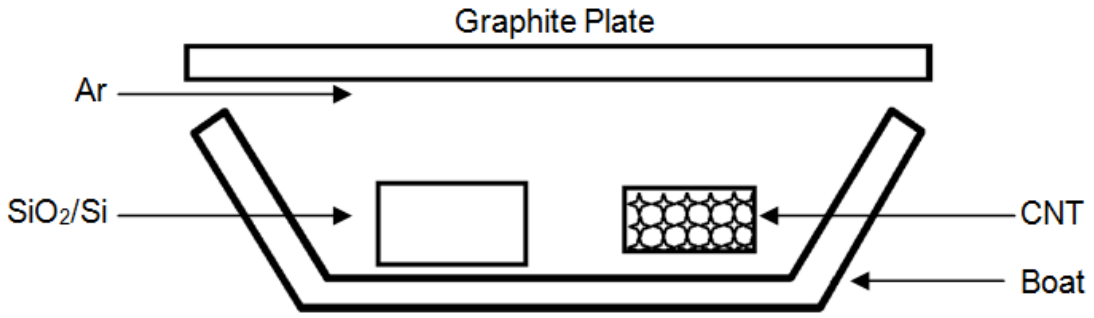

Figure 2.1 Reactor Geometry for SiC NW production from CNT and SiO_2/Si. [42]

2.1.2.2 Arc Discharge

This method gained popularity due to its capability of efficiently synthesizing CNTs in high volume. Due to structural similarities between CNTs and SiC NWs, it was believed that SiC NWs could also be synthesized in a similar manner. This belief was later proved true [45].

In this method a graphite cathode was facing an anode having a hole partially filled with a mixture consisting of graphite and Si powder[42]. At 53 kPa helium atmosphere, an arc (40A, 22V) was struck between two graphite electrodes inside a reactor filled with a 1:1 ratio of SiO_2/C mixture. The role of this arc was to vaporize the surface of cathode containing Si and C, which, when combined with already present

gaseous SiO_2/C mixture, resulted in SiC NW deposits on the other electrode. The uniformity of the NWs depends on the uniformity of the produced arc. This resulted in the formation of β-SiC whiskers with 10nm diameter. The equations 2.1 and 2.2 presented in the earlier section also apply to this method.

Although this method offers low cost and high efficiency, it has not been able to provide reliable control of the NW axis orientation. Other methods had to be explored to address this deficiency.

2.1.2.3 Laser Ablation

In this method high laser flux is applied to sublimate the material, which results in formation of free standing NW. Laser ablation is a very popular method for CNT synthesis [46][47] because the method can produce freestanding nanowires of high-purity and can be used at a low working temperature, which is important for easily-melting and multicomponent materials[42].

This method has also been used for SiC NWs. A 248nm KrF excimer pulsed laser (10Hz pulse rate)beam of energy 400 mJ per pulse was used to produced large quantity of pure SiC NWs by focusing the beam on the SiC target for 2 hours [48]. Figure 2.2 shows the setup used in [48] and Figure 2.3 shows the NWs obtained by this method. The obtained NWs had a crystalline SiC core and an amorphous silicon oxide shell, their lengths was up to tens of micrometer. The diameters ranged from 20 to 70 nm with a mean value of 55 nm. The outer shell thickness varied from 11 to 30 nm, with the mean value of 17 nm[42].

Due to significant variations of the NW diameter and high fabrication costs, other methods for SiC NW synthesis are often considered.

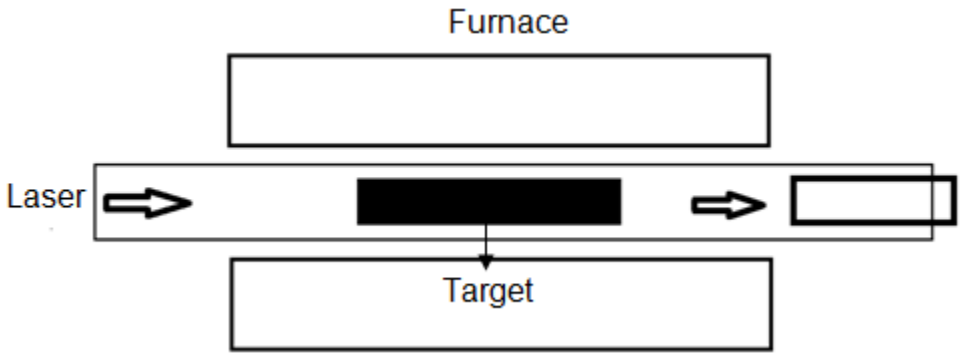

Figure 2.2 Laser ablation Scheme [42]

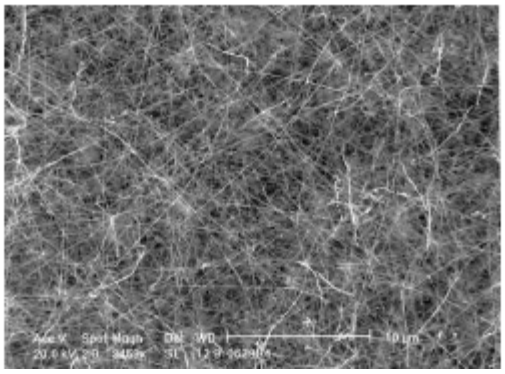

Figure 2.3 SiC NWs produced by laser ablation [42]

2.1.2.4 High-Frequency Induction Heating

This method was invented by Zhou [48] to fabricate β-SiC NWs without a catalyst. The experiments were performed in a high-frequency induction-heating furnace made of a quartz tube, surrounded by an inductively heated cylinder of graphite coated by a layer of activated carbon fibers (ACF). The procedure involved in this experiment utilizes heating of high purity SiO powder into a graphite crucible at 1450°C and 50–100 Torr .

The X-ray diffraction (XRD) pattern suggested that the synthesized coating on the surface of the graphite crucible consisted of the crystalline β-SiC with lattice constant close to standard values for β-SiC (4.359 Å) [42].

This method offers low cost, high yield and high efficiency, but its critical disadvantage is the lack of alignment. In addition, there have been no reports of any other polytypes being prepared by this method except 3C.

2.1.2.5 Chemical Vapor Deposition and VLS growth mechanism

Chemical vapor deposition (CVD) is a chemical process that is traditionally used to produce high-purity, solid thin films on crystalline substrates. This is accomplished by exposing the substrate to one or more gaseous precursors at elevated temperatures. In the case of the SiC growth, the precursors must be Si- and C-containing gasses, which react and/or decompose in the gas phase as well as at the substrate surface to produce a desired SiC film [49] [50] [51] [52].

CVD has been widely reported for NW growth (and SiC NW growth in particular). Different approaches can be used to suppress growth of a semiconductor film in favor of the NW growth. For example, vapor-liquid-solid (VLS) mechanism using nanoparticles of a metal catalyst is one of popular SiC NW growth methods. VLS is a metal-catalyst-assisted growth mechanism for the growth of one-dimensional structures by CVD. VLS mechanism was first proposed in 1964 to explain growth of silicon whiskers on silicon substrate in the presence of gold (Au) catalyst. The requirement of a catalyst to achieve 1D structures and the presence of catalyst globules at the tips of the NWs indicated the involvement of a previously unknown growth mechanism, which was named vapor-liquid-solid (VLS) mechanism [53].

VLS growth mechanism is typically described by three distinct stages:

(a) Formation of liquid metal alloy droplets, which initiates NW growth,

(b) Incorporation of the growth adatoms from the vapor by adsorption at the vapor-liquid interface, and

(c) supersaturation of adatoms in the liquid droplet and nucleation at the liquid-solid interface leading to rapid growth of a 1D structure under the metal catalyst droplet.

The main conditions, which are required to achieve and sustain successful VLS growth, are outlined below [53] [54].

1. The solubility limit of the catalyst in the liquid phase of the targeted material should be much higher than in the solid phase of the targeted material (i.e., $K = C_S/C_l < 1$, where C_S is the solubility limit in the solid phase and C_l is the solubility limit in the liquid phase). Under this condition, the catalyst easily forms a liquid alloy with the targeted material, with little contamination of the targeted material with the catalyst atoms in the solid phase.
2. The saturated vapor pressure (Vp) of the catalyst component over the liquid alloy should be small. Otherwise, the catalyst will evaporate and eventually disappear in the course of growth.
3. Metal catalyst must form a liquid solution with the component of the solid phase.
4. The metal catalyst must be inert to chemical reactions. Otherwise, a reaction could deprive it of its catalytic function.

5. The metal catalyst must not make an intermediate solid. Otherwise, the intermediate solid will also deprive it of its catalytic function.

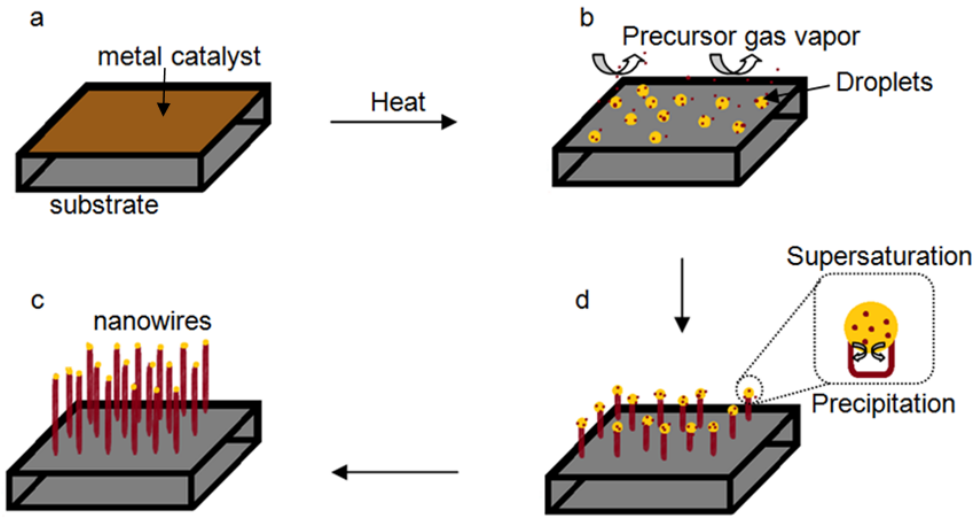

Figure 2.4 Main steps involved in growth of NW by VLS mechanism [54]

A schematic description of the main VLS NW growth steps is shown in Figure 2.4 .The first step is the formation of metal alloy droplets. When using nickel (Ni) catalyst and a SiC substrate, the metal alloy droplets are composed of nickel silicide (Ni_xSi_y). Figure 2.5 shows the ternary phase diagram of C-Ni-Si system, it clearly indicates the lack of phase in which Ni and SiC are in equilibrium. Based on the phase diagram, the reaction leading to silicide formation is the following

$$SiC + Ni \rightarrow Ni_xSi_y + C \qquad (2.5)[55]$$

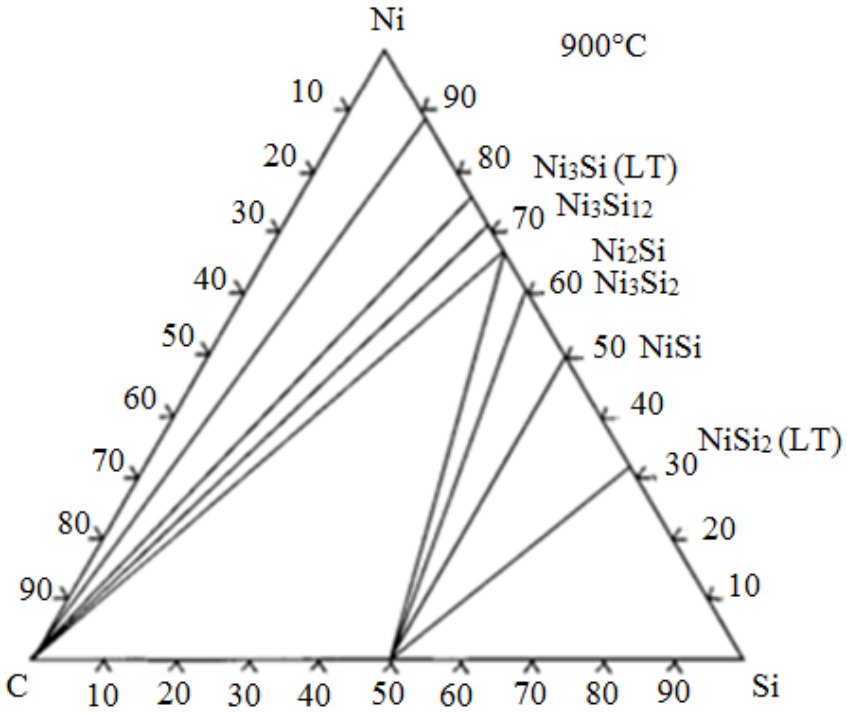

Figure 2.5 Ternary phase diagram of C-Ni-Si at 900°C [55]

This equation indicates the absence of any metal carbide, which is consistent with results of Ref. [55], where the solubility of C in Ni_xSi_y of less than 1% at around 900°C was reported. Also, according to Ref.[56], the silicide layer formations between 650°C and 1035°C follows a parabolic time dependence [55] [56] according to the equation below:

$$d^2 = 2 K_p t \qquad (2.6)\ [56]$$

where, d is the thickness of the growing silicide layer(μm), K_p is the rate constant ($\mu m^2/h$) and t is the growth time (hr).

Next, the formed silicide nanocluster melts at appropriate temperature and turns into a liquid. This liquid soon tries to attain a spherical shape due to its surface tension.

Based on the amount of contamination and/or the presence of oxide layers at the droplet/substrate interface during the experiment, the magnitude of interfacial forces (surface tension, adhesion, etc) vary.

The diameter of the NWs grown depends on the properties of the droplet alloy. The growth of nano-sized wires requires nano-size droplets. The minimum radius of a metal droplet required to achieve the VLS growth is given by

$$R_{min} = \frac{2V_l}{RT\ln(s)}\sigma_{lv} \qquad (2.7)\ [57]$$

where V_l is the molar volume of the droplet, σ_{lv} is the liquid-vapor surface energy, and s is the degree of supersaturation of the vapor.

The next step is the crucial adsorption of the adatoms from the precursor gases, which takes place at the vapor-liquid interface of the droplet. This adsorption continues until supersaturation of the adatoms in the metal alloy is reached, which prompts precipitation of the SiC at the liquid-solid interface leading to the NW growth. The different interfacial Gibbs energy changes during NW growth are reported in Ref[58].

2.1.3 Comparison of the top-down and the bottom-up approaches

Both the top-down and the bottom-up approaches have their advantages and disadvantages. The choice of which approach is to be used is primarily dictated by the application as well as by the cost considerations. Some of the merits and demerits are discussed below. Exploitation of the potential advantages of the bottom-up method for SiC NW-based electronics is the main theme of this dissertation work.

The top-down approach of NW synthesis has been used for over 50 years and experienced continuous improvement. The major problem with this approach is the

damage induced by plasma etching, which leads to a structural/chemical degradation or a phase-change in the materials. Due to high damage from etching, the reliability of the device is considerably reduced especially in the nanometer range, which in turn reduces the yield and increases the cost. There are also many engineering problems associated with this approach, for example the difficulty of achieving very long NWs of a sufficiently small and constant diameter. Solving these issues remains crucial for continued relevance of the top-down approach for nanofabrication.

As discussed earlier, the bottom-up approach is free from the disadvantages of the top-down method. However, the controllability of the NW properties is the major issue that needs to be addressed. Even though extensive work has been done to control specific parameters such as polytype, density, thickness, orientation, more research is required to consistently control all these parameter.

2.2 The current status and problems of SiC NW growth

Portions of the following chapter are reprinted with the permission from B. Krishnan, R. V. KG Thirumalai, Y. Koshka, I. Levin and A. V. Davydov, "Substrate-dependent orientation and polytype control in SiC nanowires grown on 4H-SiC substrates," Crystal Growth & Design, Vol. 11, No. 2, 2011, 538-541.

The previous work on SiC NWs synthesis predominantly relied upon the VLS growth mode. The list of reported synthesis techniques includes reaction of carbon-source gases with Si substrates [59], pyrolysis of powders containing the source materials[60], [61], reaction of source gases with carbon nanotubes [62], microwave heating-assisted physical vapor transport[63] and chemical vapor deposition (CVD).[64], [65].

Various substrates have been used for SiC NW synthesis, including SiO_2[30], [65], graphite[60][61][62][63], poly-SiC [64], etc. Only a few attempts to utilize monocrystalline 6H [67] and 4H [7], [30], [64–66], [68–70] SiC substrates have been reported. The use of monocrystalline SiC substrates offers a promise of polytype control in SiC NW growth, however only a limited progress in this direction has been achieved so far.

As was mentioned earlier, polytype control and crystallographic orientation of NW axis are crucial for utilization of SiC NWs in electronic devices. While polytypes of NWs grown by different techniques have been extensively investigated, the previously developed capabilities for the polytype control are limited. SiC NWs commonly crystallize in the 3C polytype. Different crystallographic orientations of the 3C NW axis have been reported, including ⟨111⟩ [7], [64], [65], ⟨110⟩, ⟨100⟩ [68] and ⟨112⟩ [68]. Relatively rare observations of other polytypes include 6H [40], [60], [61], [64], [67], 2H [64], [69], and 15R [64][66]. Only a few studies have reported traces of the 4H polytype.[66], [71].

A successful attempt to utilize 6H-SiC substrates for achieving substrate-dependent NW alignment was reported in Ref. [67]. Evidences for the dominance of the 6H polytype have been provided.

No information exists about substrate-determined preferential orientations and the dominant polytypes of NWs grown on 4H SiC substrates.

CHAPTER III

EXPERIMENTAL APPROACH

In this work, we employed a horizontal hot-wall chemical vapor deposition (CVD) reactor for the NW growth experiments. This reactor was previously used to demonstrate SiC NW growth feasibility on a 4H-SiC substrate[70][72]. These feasibility experiments also yielded optimum growth parameters including the growth temperature, C/Si ratio, catalyst choice etc. The obtained growth conditions and the experimental setup served as the starting point for my work are briefly discussed below.

3.1 CVD setup for SiC NW growth experiments

3.1.1 CVD Reactor

The most crucial component of the experimental setup used in this work is the CVD reactor. It includes a chamber in which chemical reactions take place under high temperature and controlled pressure. The schematic diagram of the horizontal hot wall CVD chamber used in our experiments is shown in Figure 3.1.

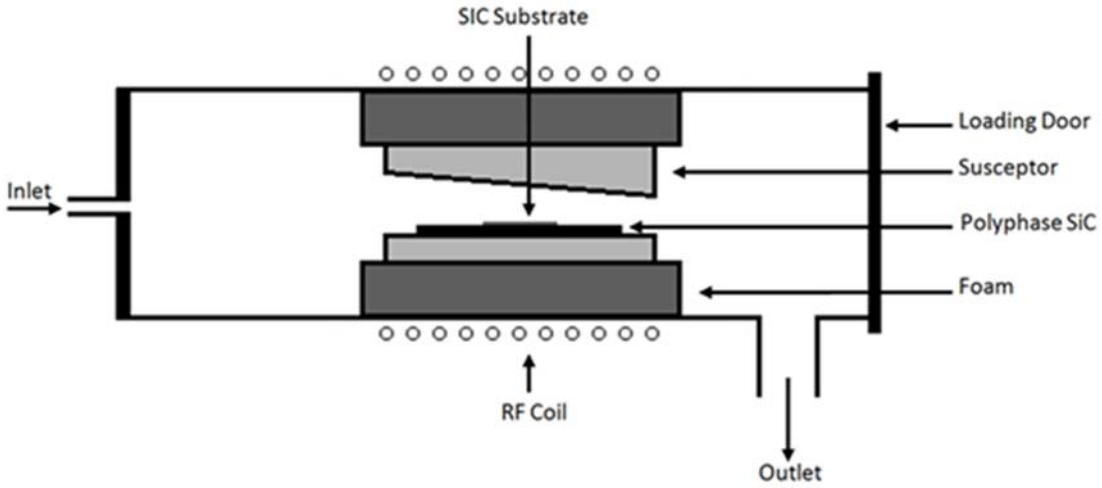

Figure 3.1 Two Dimensional view of Horizontal Hotwall CVD reactor

The chamber consists of an airtight quartz tube surrounded by a RF coil, thermal insulating foam, susceptor, and a wafer carrier. The susceptor inside the reactor chamber is heated by applying a high-frequency voltage to the RF coil. High temperature inside the susceptor opening facilitates chemical reactions responsible for the CVD growth. Accuracy and reliability of the temperature control is very important. Drilling a hole in the ceiling of the susceptor halfway through and focusing the optical pyrometer on the hole ensured reliable growth zone temperature measurement. The susceptor was made of graphite and was coated with a SiC layer to suppress out-diffusion of impurities at elevated temperature. It was placed inside a thermal insulating foam and had an opening inside to hold the warier carrier with the sample and to allow passage of the reactive gasses.

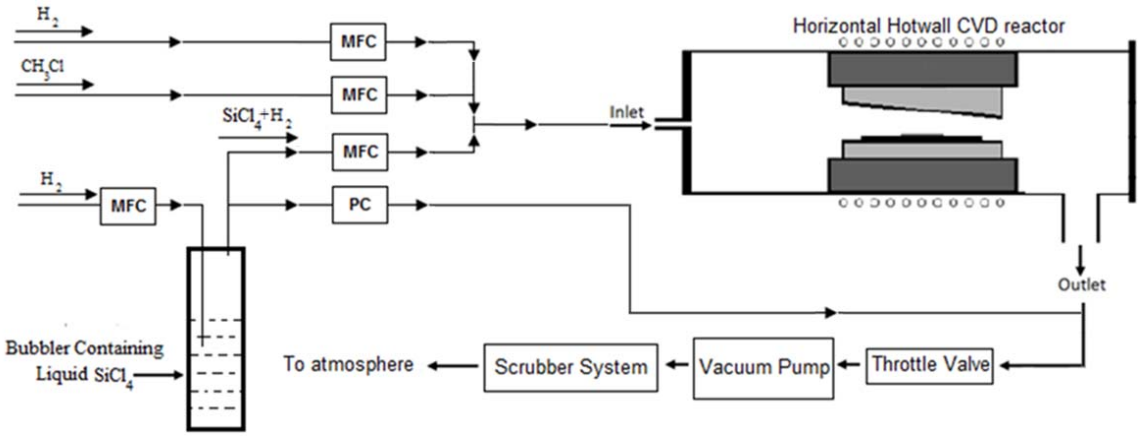

Figure 3.2 Schematic of the CVD system setup used for the experiment

The gases used in our experiment were chloromethane (CH_3Cl), silicon tetrachloride ($SiCl_4$) and hydrogen (H_2). H_2 was a carrier gas. CH_3Cl and $SiCl_4$ acted as silicon and carbon sources respectively. The $SiCl_4$ is supplied in a liquid form and requires a bubbler setup shown in Figure 3.2.

3.1.2 Sample Preparation

The objective of the study was to investigate the NW growth mechanisms and establish some of the main factors influencing the NW density, polytype control and the orientations of the NW axis with respect to the substrate. The samples and their preparation method varied widely based on the specific objectives.

3.1.2.1 Bare 4H-SiC Substrates

All bare 4H-SiC substrates (8° off-axis) were cleaned using ultrasonic shaking in acetone, isopropanol, and deionized water before each growth run to remove of all the possible organic and inorganic contaminants. The cleaned samples were then placed on a wafer carrier at the center of the graphite susceptor for the growth run.

3.1.2.2 4H-SiC Substrates with Metal Catalyst

4H-SiC substrates with nano-particles of a metal catalyst for VLS-based growth were formed by deposition of Ni or NiSi layers of varying thickness by sputtering on bare 4H-SiC substrates. In some cases the metal catalyst layers were patterned using plain lift-off photolithography to ensure that only certain regions of the substrate are covered with the catalyst. The samples were then cleaned in a similar manner as the bare 4H-SiC substrates before the growth run.

3.1.2.3 4H-SiC Mesas

In addition to bare SiC substrates and metal catalyst covered (0001) top surfaces of the substrates, 4H-SiC mesas were used to investigate preferential orientations of NWs grown on different crystallographic surfaces and a possibility of growing on patterned surfaces. These mesas (Figure 3.3) were formed by reactive ion etching (RIE) with a 9:1 ratio of SF_6/O_2 at 70 mTorr using Ni as an etch mask. The resulting mesas were between 10 and 17 μm tall.

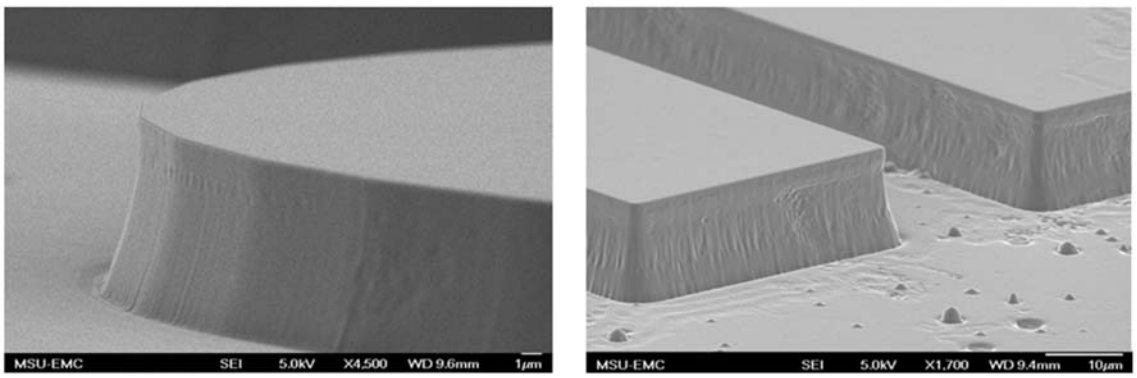

Figure 3.3 Mesa on 4H-SiC 8° off-axis substrate to analyze preferential orientation

3.1.3 Growth Conditions

The growth conditions such as temperature, pressure, duration and precursor flow rates were varied to identify the optimum condition for NW growth. The temperature was varied between 900°C and 1175°C at pressure of 140Torr. The growth duration was varied from 7 min to 30min primarily to control the NW length. Specifics of the growth conditions and the reasoning behind selecting those conditions will be discussed in detail in the upcoming chapters.

3.2 Metal contact fabrication for measuring electrical properties

3.2.1 Photolithography-based patterning and contact deposition

In order to investigate electrical properties of the grown NWs, a standard approach to forming metal contacts (without using e-beam lithography) was attempted. The basic flow of steps towards forming metal contacts using regular optical lithography is as follows.

1. Deposit the 1st metal layer and define the electrode pattern using conventional photolithography;
2. Harvest SiC NWs from the growth substrate. It was done by ultrasonic treatment of the sample in a solvent solution;
3. Disperse a drop of the NW solution onto the dielectric substrate. The substrate was a Si wafer covered with a thermally grown SiO2 layer for electrical isolation. Use of the AC electric field during NW dispersion from the solution (di-electrophoresis) was investigated to achieve NWs better aligned between the given pair of electrodes. The di-electrophoresis

approach was adopted and tried, however it needs to be optimized to cause any improvement in the alignment of SiC NWs.

4. Let the solution dry, resulting in NWs resting on the dielectric surface. Some fraction of the NWs is expected to end up located between some pairs of the electrodes.
5. Deposit and pattern the 2nd (top) layer of the metal electrodes. The metal is selected thick enough to be used with a probe stand or wire-bonder. The two ends of the NW are sandwiched between the 1st and the 2nd metal layer.
6. Form the bottom Ohmic contact.

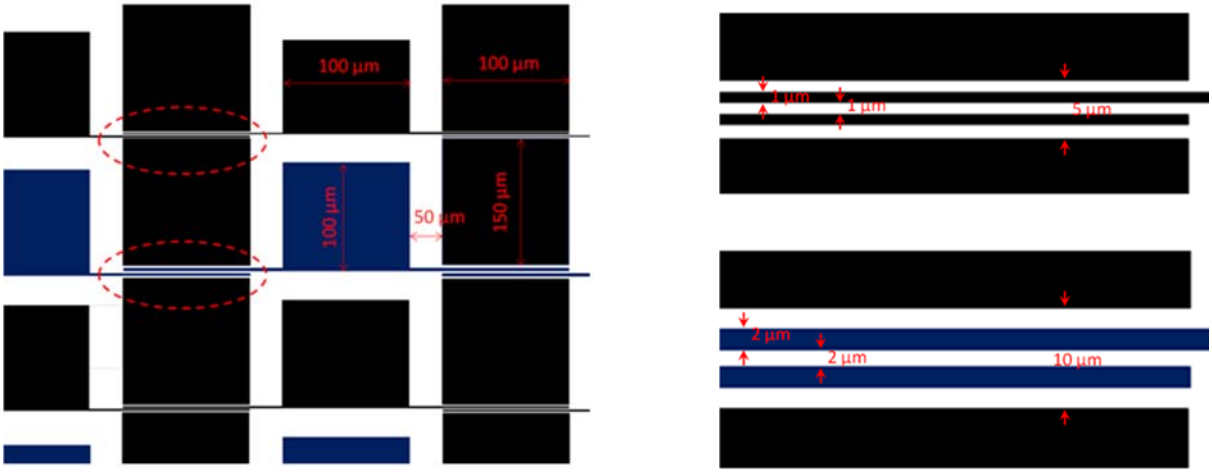

Figure 3.4 The photolithography mask designed to provide 4-point contacts for SiC NWs. NWs were deposited from the solution and an alignment attept using a di-electrophoresis was conducted. The right figure shows a magnified view. Two different spacings and widths of the metal contacts were designed.

Figure 3.4 shows the pattern of the photolithography mask that was designed to fabricate the 2nd metal layer (the top layer). The 1st - layer mask (not shown) included only large square regions (contact pads), having slightly smaller dimensions to provide some margin for the alignment error, while not including the thin lines serving as 4-point-probe contacts.

Metal deposition and patterning of the first-layer contacts using the first mask was conducted. The pattern was used for di-electrophoresis deposition of the NWs, when electric field is applied to the NW through the solvent and causes NW alignment with respect to the contacts to which the electric field is applied. After the NW deposition was completed, only small number of NWs end up having desirable alignment and none would be properly positioned to connect two metal contacts. Furthermore, the density of the NWs in the solution should be controlled to avoid deposition of multiple NWs at the same pair of contacts. The work in this direction did not yield convincing results to continue efforts in this direction. Instead, formation of metal contact to individual SiC NWs using FIB metal deposition was attempted as described in the next section.

3.2.2 Focused Ion Beam (FIB) assisted Deposition

FIB is a technique widely used in semiconductor industry. It often combines SEM and FIB capability. It offers metal deposition and sample etching capabilities, in addition to imaging. FIB uses a focused beam of ions (mostly Ga^+) while the SEM uses a focused beam of electrons to image the sample. FIB systems may have both electron and ion beam columns, allowing the same area to be imaged using either of the beams. Unlike SEM, FIB is inherently destructive to the specimen since high-energy ions striking the surface sputter the atom from surface of the sample.

FIB- induced deposition is performed by introducing a gas containing the metal to be deposited into the vacuum chamber, which is followed by scanning the area with ion beam where metal needs to be deposited. In the scanned area the precursor gas will decompose into volatile and non-volatile components; the non-volatile component, chemisorbs on to the surface. Many materials such as tungsten, platinum, cobalt, carbon, gold, etc., can be selectively locally deposited using FIB.

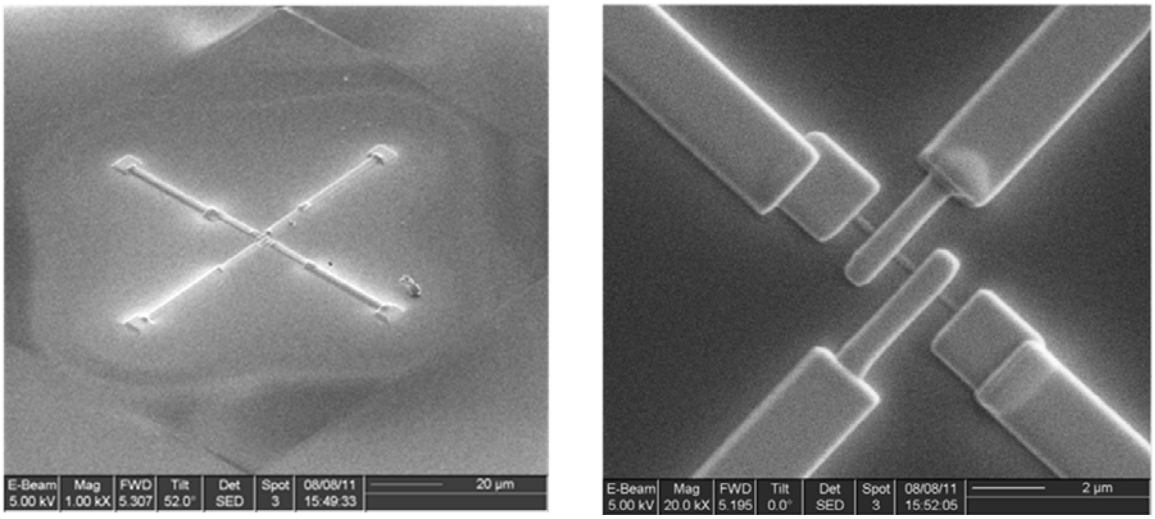

Figure 3.5 SEM images of the metal contacts to an individual SiC NW for the four-point-probe measurements of the NW conductivity (Left) the full view and (Right) the magnified view. The contacts were made by the focused ion beam (FIB) direct-write technique.

In this work, FIB was used to form small contacts to SiC NWs for electrical characterization. SiC NWs were harvested om the growth substrate using the procedure described in section 3.2.1. The NWs were randomly dispersed onto the SiO_2-covered surface of a Si wafer. An individual NW of sufficient length (4-5 µm) was found by searching through the substrate area under SEM. Using FIB, four platinum electrodes

were deposited contacting the NW (Figure 3.5). Following the FIB deposition, sufficiently large metal pads suitable for the probe stand or wire bonding were fabricated by a conventional photolithography. Photoresist at the desirable region of the sample (contacting the end of one of the metal contact lines) was exposed through the circular windows in the mask. Contact pads to the other three FIB-fabricated contact lines were made using the same procedure (Figure 3.6).

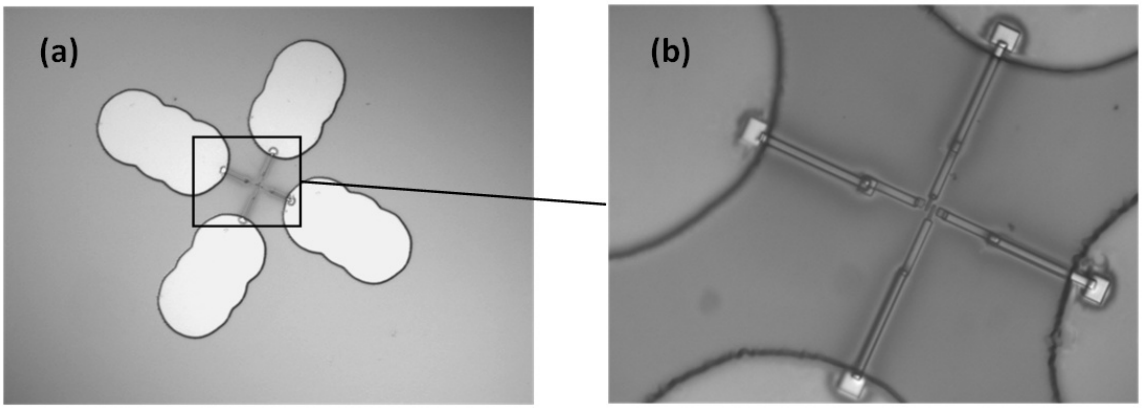

Figure 3.6 Optical micrographs of the SiC NW test structure with 4 contacts made by FIB-deposition and large contact pads fabricated by the conventional photolithography: (a) the full view and (b) the magnified view. The images were taken after the photoresist development prior to the metal deposition and lift-off.

3.3 NW characterization

The grown SiC NWs were characterized using various characterization techniques to establish their polytype, crystalline quality and compare their properties at different growth conditions. The techniques used for characterization included Nomarski optical microscopy, scanning electron microscopy (SEM), energy dispersive spectroscopy

(EDS), powder X-ray diffraction (XRD), and selected area electron diffraction (SAED). The techniques used and the information they offer are briefly discussed below.

3.3.1 Nomarski optical microscopy

Nomarski or differential interference contrast (DIC) optical microscopy allows the user to examine low contrast samples and achieve higher contrast in bright field illumination. This technique was used in this work to qualitatively examine the effect of the growth conditions on NW growth and also to estimate changes in NW density and distribution. The Nomarski microscope uses a single DIC prism placed in between the objective lens and the light reflector. The DIC prism serves two purposes of splitting the incident beam and recombining the reflected beam. This setup creates two different light paths which facilitates the creation of prism interference in the image plane between the two slightly displaced images, thus producing height contrast.

3.3.2 Scanning Electron Microscopy (SEM)

Scanning electron microscopy (SEM) is a type of electron microscope that is used to image samples with an electron beam. The basic working of the SEM involves creation of electron beam by application of a high voltage to the filament of a cathode ray tube, which facilitates the thermionic emission of electrons. The electrons are then accelerated towards the sample under investigation. Multiple coils focus the electron beam onto the sample. This focused electron beam is deflected to raster scan the whole surface of the sample. The interaction between the electron and the sample surface produces signals from secondary electrons etc, which is used to image the samples topography accurately. In our study SEM is used to examine the NWs surface and measure their dimensions.

3.3.3 Energy Dispersive Spectroscopy (EDS)

Energy-dispersive X-ray spectroscopy (EDS or EDX) is an analytical technique used for the elemental analysis of a sample. This technique is an attachment to our SEM. It also relies on the interaction of the electron beam with the sample. Since each element has a unique atomic structure, each material gives a unique set of peaks in their X-ray spectra. The basic idea behind EDS is that when an incident electron beam excites an inner-shell electron dislodging it, an outer shell electron of higher energy fills its void releasing the difference in energy between shells as X-ray. Energy detector records this emitted X-ray spectrum, and the observed peaks in X-ray spectrum is used to uniquely identify the elements. Thus, this method allows us to conduct the elemental composition analysis of any specimen, which in our case is the NWs and the metal droplets used as the VLS growth catalyst.

3.3.4 Electron Backscatter Diffraction (EBSD)

Electron backscatter diffraction (EBSD) is a technique used to obtain crystallographic information by analyzing the pattern formed by backscattered electrons from the sample. Backscattered electrons are the high energy elastically scattered electrons which are reflected by the specimen interaction volume when the electron beam hits the specimen. This is also an attachment to SEM or FIB. This technique can be used to analyze the specimen orientation and phases by matching the obtained EBSD pattern with theoretical simulations. It was used in this work to confirm the polytype of the NW.

3.3.5 Powder X-ray Diffraction (XRD)

X-ray diffraction is a non-destructive technique commonly used in material characterization. Determination of crystal structure, composition, orientation, and phase identification of materials are among some of powder XRD's capabilities.

In our study, verification that grown NWs are indeed SiC and rapid (though preliminary) identification of their polytype was accomplished using powder XRD. Constructive interference of monochromatic X-ray forms the basis of any X-ray diffraction technique. The first step in creating a monochromatic X-rays is applying a high voltage to the cathode ray tube containing a heating filament usually made of tungsten. When sufficiently high voltage is applied to the filament, electron emission takes place, which is directed towards a high-density target material. X-rays emission occurs when sufficiently high-energy electrons dislodge the inner shell electrons of a target material. This X-ray is filtered and directed towards the sample to be examined. The interaction between the incident X-ray and the sample produces constructive interference based on Bragg's Law ($n\lambda=2d\sin\theta$). By analyzing the angle of incidence and the counts of the detected diffracted X-rays and comparing then with the available reference data, we can identify the chemical composition of the unknown sample or ascertain the crystal properties of the samples including the polytype.

3.3.6 Transmission Electron Microscopy (TEM) and electron diffraction

Transmission electron microscopy (TEM) is a microscopy technique where an electron beam is transmitted through an ultra thin specimen (<1μm). The interaction of the electron beam with the material is studied revealing the properties of the specimen.

TEMs have higher resolution compared to other microscopy owing to smaller de Broglie wavelength of electrons.

TEM can be used to obtain topographical, morphological, compositional, and crystalline information of a specimen. Crystal structure of the specimen can be identified using one of the TEM-based techniques known as selected area electron diffraction (SAED). We are particularly interested in SAED diffraction patterns because they enable identification of the SiC polytype. The three basic steps involved in polytype identification using SAED are:

1. Preparation of the sample for TEM by thinning the specimen. Thinning the specimen to less than a micron is needed to allow transmission of the e-beam.
2. Calibration of TEM to obtain camera constant.
3. Obtaining a diffraction pattern using TEM.
4. Calculation of the distance between planes (d-spacing) and the angle between the planes of the expected crystal.
5. Matching the theoretically calculated D-spacing and the angle between planes with the observed ones obtained from TEM. If they match, the diffraction spots are indexed with their miller indices and thereby the SiC polytype of the specimen is identified. The axis normal to all planes seen as diffraction spot is the zone axis found by a simple cross product.

Figure 3.7, Figure 3.8, Figure 3.9 and Figure 3.10 show results of one such indexing effort aimed at identifying the polytype of a SiC NW grown in our lab. The results showed the domination of 4H-SiC polytype with 3C inclusions.

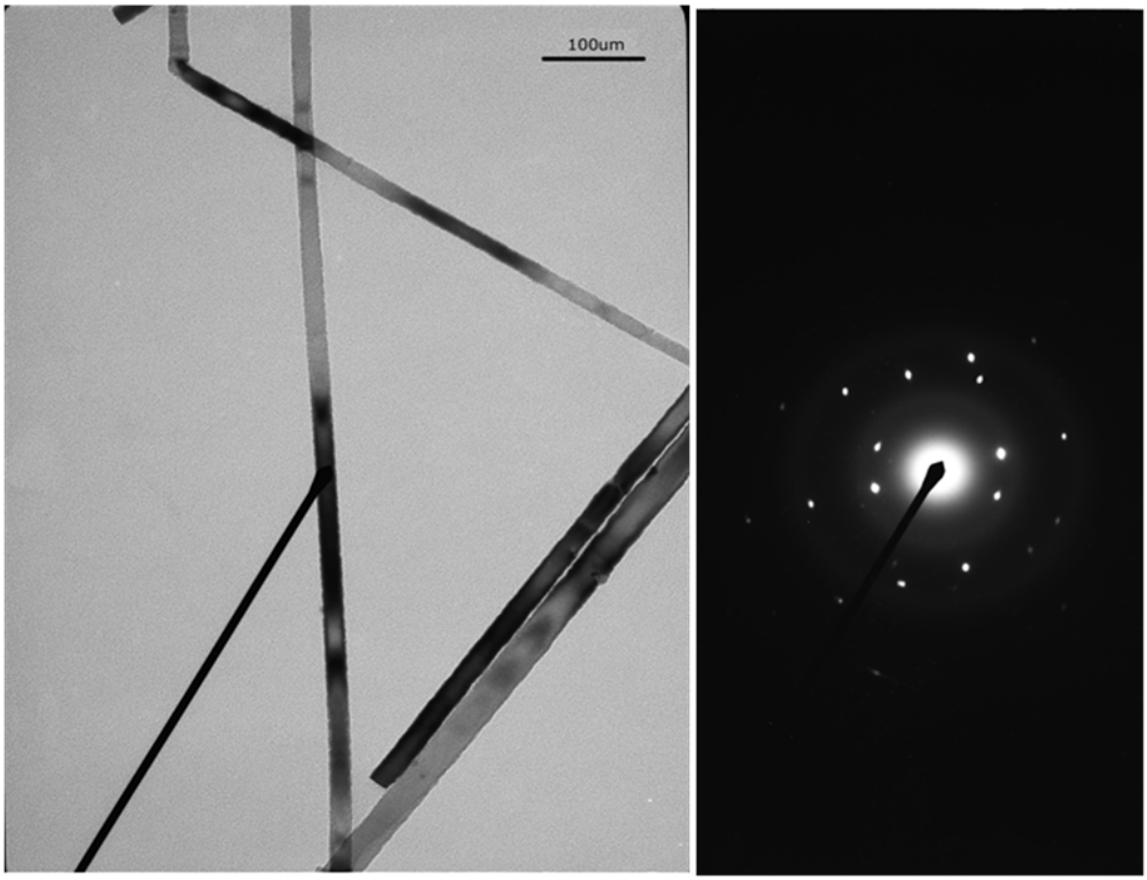

Figure 3.7 TEM image of a nanowire at 100,000X (left) and its corresponding diffraction pattrn obtained with the camera length of 40 cm (right)

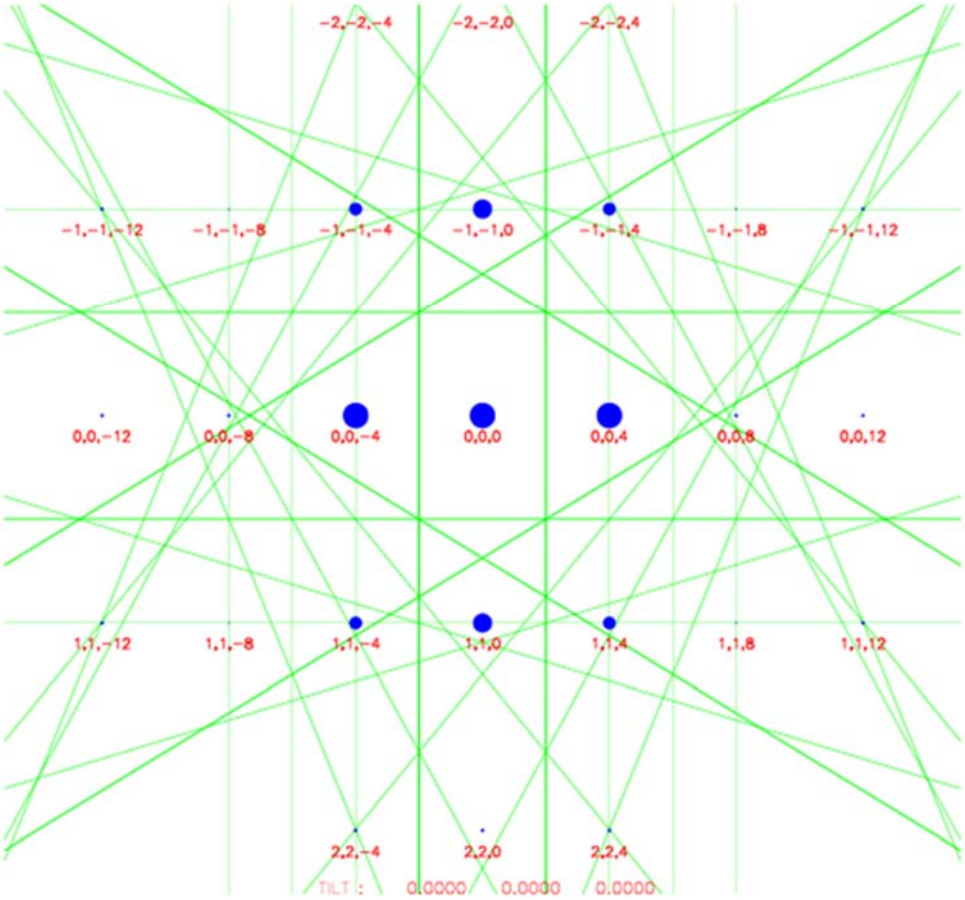

Figure 3.8 Expected diffraction pattern for 4H-SiC with zone axis [1-10] [73]

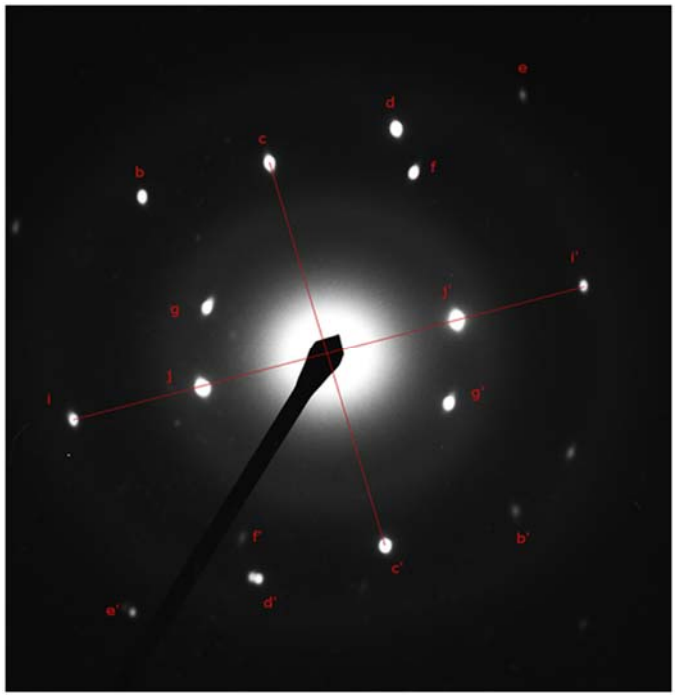

Figure 3.9 Indexed diffraction pattern of Figure 3.7

		Camera Const, λL = 1.6784695 nm mm					
Spots	D(mm)	R(mm)	d=λL/R(A)	Expected d-spacing for 4H-SiC[60]	Observed angle w.r.t horizontal (Θ)	4H Spots	3C Spots
cc'	21.6	10.8	1.554138426	1.54	-74.2	-1-1 0	
bb'	25.1	12.55	1.337425896	1.314054	-42.42	-1-1-4	
gg'	13.2	6.6	2.543135606		-23.68		111
ii'	26.5	13.25	1.266769434	1.26	15.92	00-8	
jj'	13.2	6.6	2.543135606	2.52	16.17	00-4	
ee'	34.1	17.05	0.984439589	0.975186	235.36	-1-18	
ff'	21.6	10.8	1.554138426		246.61		0-22
dd'	25.3	12.65	1.32685336	1.314054	254.17	-1-14	

Figure 3.10 Snapshot of calculations involved in indexing of the diffraction spots

3.3.7 Electrical Characterization

The experimental set-up for performing current voltage (I-V) measurements used Keithley 237 I-V meter. The I-V meter was connected to a computer using GPIB to USB converter and controlled using LabView. The four-point probe structure of a SiC NW on a Si substrate was wire-bonded on a 24 pin DIP package. The I-V meter was programmed to plot I-V curves, and the plots were later used to extract conductivity and estimate carrier concentration. The details of the acquired data and the analysis will be presented in detail in the Results section.

CHAPTER IV

EXPERIMENTAL RESULTS AND ANALYSIS

4.1 Previous work - NW growth with Au and Ni

Ref.[70] and Ref.[72] report the initial work done at MSU on SiC NW growth using 4H-SiC substrate. That work served as the starting point for the NW growth experiments covered in this dissertation and those results were used to select the metal catalyst and identify the process window suitable for SiC NW growth using VLS mechanism. The objectives and results of that preceding work are briefly discussed below with a goal of providing a proper context for the experiments conducted in the present dissertation work.

4.1.1 Previous work: Objectives and the experimental approach

The main objective of the initial work on SiC NW growth conducted in our group [70] ,[72] was to develop a basic process for SiC NW growth in the epitaxial reactor at Emerging Materials Research Laboratory (MSU). This process was to be used in the subsequent work (i.e., this dissertation work) to explore polytype control in SiC NWs grown on 4H-SiC substrates.

The growth substrates used included a 5nm thick layers of a metal catalyst deposited on a 10x10 mm square piece of n-type 4H-SiC substrates with a vicinal cut of 8^{o} towards [11-20] direction. Gold (Au) and nickel (Ni) were the two metal catalysts

chosen to explore the VLS growth mechanism. Following the metal layer deposition by e-beam evaporation, the metal catalyst layers were subjected to various heat treatments (including the in-situ treatment during the heating of the sample in the epitaxial reactor prior to NW growth) to induce nano-particle separation by dewetting. While the pre-treatment conditions are expected to influence the droplet size and consequently the NW diameter, no effect of the attempted treatment was established in this work. Actually, the in-situ treatment was adequate for the targeted objectives.

The growth experiments used hot-wall CVD reactor and were conducted at 150 Torr with H_2, $SiCl_4$ and CH_3Cl as the carrier gas, silicon source and carbon source respectively. This work had two main objectives: (a) selection of a suitable metal catalyst and (b) identification of a temperature range favoring VLS growth while suppressing the regular epitaxial SiC film growth. There was no focused attempt to achieve epitaxial relationship between NWs and the substrate.

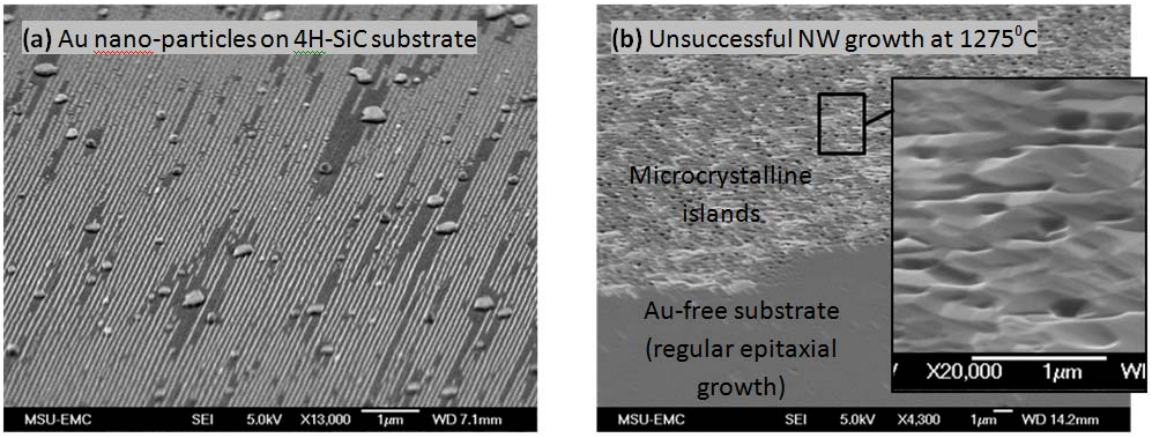

Figure 4.1 (a) 4H-SiC substrate covered with Au nano-particles, which were used to enable VLS mechanism for NW growth, and (b) a result of an unsuccessful growth attempt at 1275°C – too high growth temperature resulted in formation of microcrystalline islands due to early degradation of metal nano-particles. A region of the 4H-SiC substrate free from the metal catalyst experienced regular epitaxial growth. [70]

4.1.2 Previous work: Results of the Initial experiments – Ni and Au catalysts

4.1.2.1 The range of the growth temperature favoring VLS growth

A suitable growth temperature (Tg) range is very crucial for any growth process. The growth temperature conditions for this work were found by varying Tg and qualitatively studying NW growth. At a preselected precursor flow, pressure, etc, temperatures above 1200°C were found to be favoring epitaxial growth of a SiC film rather than VLS growth of NWs for both Ni and Au metal catalysts. When reducing the growth temperature to achieve VLS growth, the precursor flow rates also had to be reduced. These process modifications finally resulted in successful NW growth for both metal catalysts in a temperatures range from 1050°C to 1150°C. In addition, the precursor flow rates were found to directly affect the growth rate at 1150°C

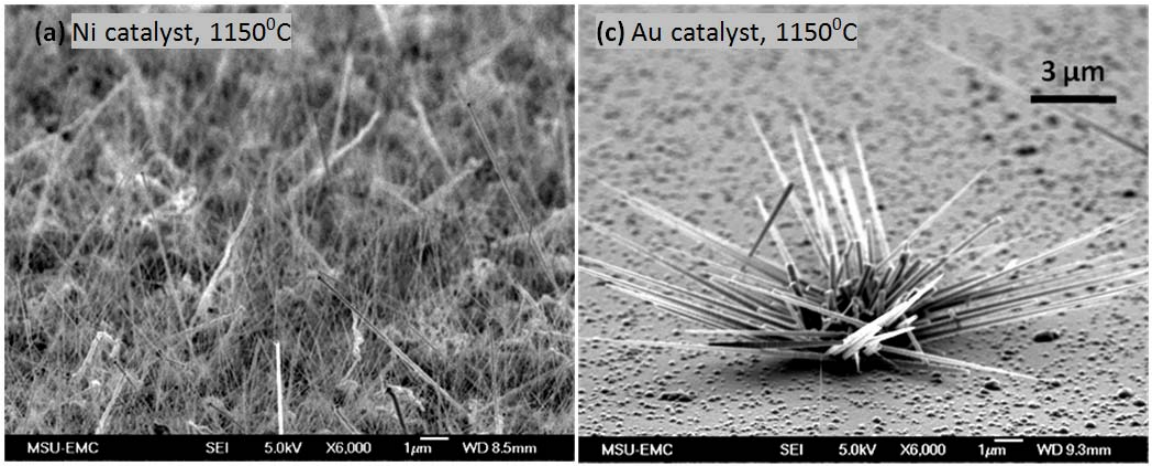

Figure 4.2 (a) SiC NWs grown with Ni metal catalyst at 1150^{0}C (b) Bushes of SiC NW grown with Au metal catalyst at the same flow conditions [59]

4.1.2.2 Comparison of the density of the grown NWs

In the case of Au metal catalyst, reduction of Tg down to 1100 and 1050°C caused (1) transition from isolated NW "bushes" to more homogeneous distribution of NWs, and (2) reduction in the diameter of the nano-fibers down to below 100 nm. However, only relatively large Au nano-particles contributed to sustainable NW growth, resulting in a relatively rare individually standing NWs at 1050°C.

In the case of Ni catalyst, reducing the growth temperature down to 1150°C resulted in successful NW growth (Figure 4.2). Dense arrays of randomly oriented NWs with diameters ranging from close to 100 nm (rare) to below 10 nm were achieved at 1150^{0}C. Further reduction in the growth temperature down to 1100°C showed the trend of thin and more homogeneous NW diameters. The length of the NWs grown in this range of the growth temperatures and growth conditions was around 10μm after a 15-min growth run.

Figure 4.2 compares the results of SiC NW growth at 1150°C using Ni and Au catalysts. The comparison clearly showed that Ni catalyst provided much more homogeneous and dense NW growth density compared to Au catalyst when used at the same precursor flow and temperature conditions. The origin of the observed differences between the two attempted catalyst metals has not been further investigated.

After analyzing the results of Ref.[70] and Ref.[72], Ni was selected as the main catalyst based on the flexibility and convenience it offered to achieve the goals of this dissertation.

4.2 Vapor-phase catalyst delivery as a new method for SiC NW growth

Portions of the following chapter are reprinted with the permission from R. V. K. G. Thirumalai, B. Krishnan, A. V. Davydov, J. N. Merrett and Y. Koshka, "SiC nanowire vapor–liquid–solid growth using vapor-phase catalyst delivery," Journal of Materials Research, Vol. 28, No. 1, Jan 14, 2013, pp 50-56, doi:10.1557/jmr.2012.208.

4.2.1 Description of the experimental arrangements

The NW growth experiments in this work [74]were conducted in the same hot-wall CVD reactor designed for epitaxial growth of SiC that was used in Ref.[70] and Ref. [72]. The growth was conducted at 1150°C and 150 Torr using H_2, $SiCl_4$ and CH_3Cl as carrier gas, silicon source and carbon source, respectively. Commercially available 8° off-axis n-type 4H–SiC (0001) substrates were used in most of the experiments. Ultrasonic shaking in acetone, isopropanol, and DI water before the growth run was used to clean the samples. The samples were then placed inside the opening of the hot-wall susceptor in the reactor. After establishing the target pressure with H_2 flow, the

temperature was ramped to 1150°C in 10−15 min. The growth run was initiated by establishing the desired flows of the silicon and carbon precursor. The growth time was adjusted to obtain a desired NW length most convenient for investigating the growth orientation, which was estimated from the NW length obtained after a 30 min run at the given growth conditions.

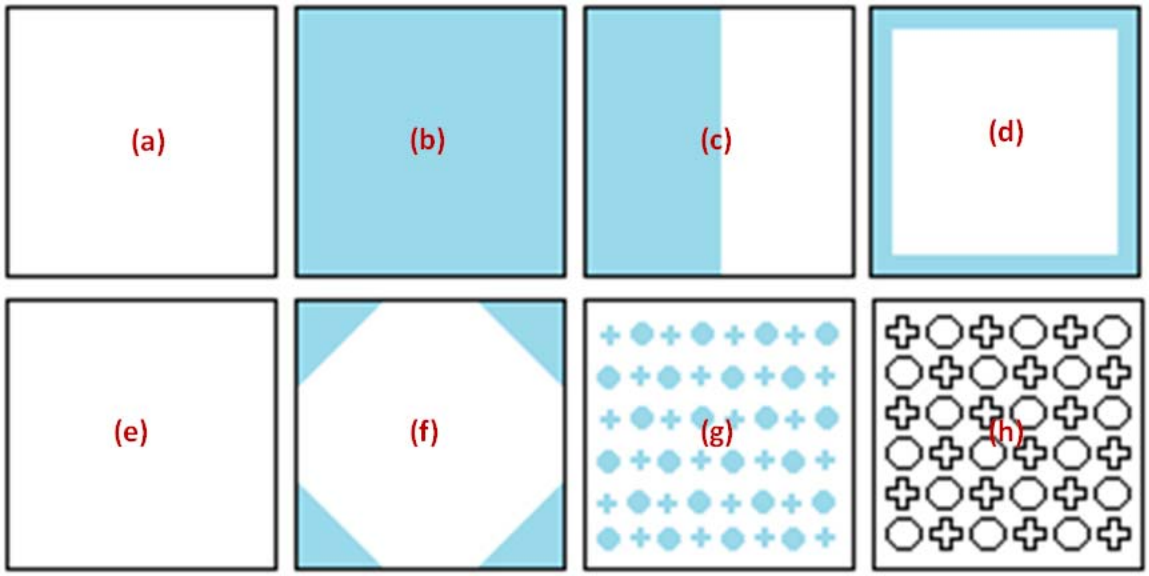

Figure 4.3 A schematic illustration of the different types of 4H-SiC substrates used during "vapor phase catalyst delivery" study: (a) Catalyst-free 8° off-axis 4H-SiC substrate, (b) 8° off-axis substrate with fully blanketed metal catalyst (Ni/NiSi), (c) 8° off-axis substrate, half sputtered with NiSi, (d) 8° off-axis substrate with NiSi covered edges (e) On-axis substrate without any catalyst. (f) 8° off-axis substrate with NiSi covered corners. (g) 8° off-axis substrate with a NiSi pattern. (h) 8° off-axis substrate with mesas formed by Reactive Ion Etching (RIE) (no catalyst).

4.2.1.1 Experimental conditions for the growth with a catalyst layer deposited on the substrate surface

In the initial experiments, Ni was blanket deposited on the growth substrates to promote VLS growth since Ni was found to provide a more favorable distribution of

NWs at the surface compared to Au (see discussion in section 4.1.2.2). As an alternative (or an improvement) to Ni, NiSi layers were also used. The NiSi layers with the thicknesses around 2000 Å were deposited by sputtering in Ar from a NiSi target. However, it should be mentioned that no detectable differences could be established in this work between NWs grown using Ni or NiSi polytype.

In addition to having the entire surface of the sample covered with the catalyst layer, some of the substrates covered with a blanket-deposited layer of Ni or NiSi films were also patterned to produce a certain fraction of the substrate surface not covered with the catalyst (Figure 4.3). The patterned catalyst layers were formed by using a conventional photolithography and lift-off.

4.2.1.2 Experimental conditions for the growth with a catalyst present only on a separate sample

Some experiments utilized an entire substrate free from a catalyst. To ensure the VLS growth mechanism, a catalyst source in the form of a separate piece of a SiC sample covered with a NiSi layer (i.e., a catalyst source) was placed 1−2 mm upstream from the catalyst-free NW growth substrate. In this arrangement, the NW growth was expected to occur due to a vapor-phase catalyst transfer from the catalyst source to the SiC substrate. The distance between the catalyst source and the SiC substrate was varied to qualitatively identify the extent of the catalyst transfer from the source and understand how the distance between the catalyst source and the growth substrate affects the NW density.

In one of the experiment, the NW growth was conducted on a 4H–SiC substrate covered with a polycrystalline SiC layer to investigate the influence of the substrate surface on the vapor-phase catalyst transfer and condensation. In addition, in order to

investigate the potential of the vapor-phase catalyst delivery for growing on patterned surfaces, 4H–SiC mesas of varying dimensions were used. The process involved in forming these mesas is discussed in section 3.1.2.3.

4.2.2 Evidences for the in-situ vapor phase catalyst delivery

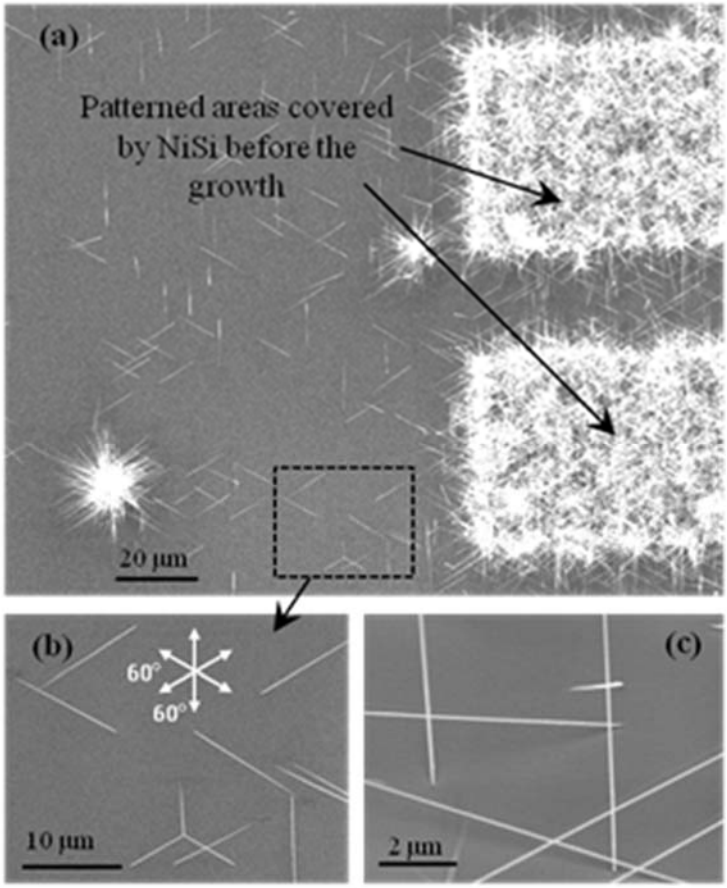

Figure 4.4 (a) A SEM top view of SiC NWs growing on the (0001) surface of a 4H–SiC substrate in the regions covered with NiSi catalyst as well as on the not covered surface by the vapor-phase catalyst delivery mechanism. (b) and (c) show magnified top and tilted (20° tilt) views showing substrate-dependent orientations of the NWs growing by the vapor-phase catalyst delivery mechanism. In addition, some bushes of misaligned NWs can be observed in (a).

4.2.2.2 Growth in regions free from the catalyst layer

The growth experiments were performed using conditions that were previously developed to grow SiC NWs on substrates covered with the metal catalyst layer (i.e., growth by the regular seeded catalyst method). Whiter regions in Figure 4.4 (a) correspond to catalyst-layer-covered regions and show growth of dense SiC NWs similar to what we observed in Ref.[70], [72]). In addition, a significant number of NWs (even though at a lower density) was also found in regions on the substrate that were not originally covered with the catalyst (Figure 4.4). Apparently, this secondary growth proceeded due to a vapor-phase transfer of the catalyst from the catalyst-layer-covered areas to the catalyst-free regions of the substrate. Energy-dispersive x-ray spectroscopy (EDS) analysis confirmed the presence of Ni in the metal droplets at the tips of the NWs grown in the catalyst-free regions. The chemical composition of the metal droplet was similar to that measured from the metal droplets in NWs produced by the regular seeded catalyst method.

Closer look at the catalyst-free areas (Figure 4.4 (b) and (c)) revealed that the NWs grow epitaxially with their axes aligned at certain direction with respect to the substrate. The NW axes alignment is investigated in section 4.3. XRD and EDS results were very similar to those reported for NWs produced by the regular seeded catalyst method and confirmed that only SiC NWs were formed. It should be mentioned that achieving such low NW density was very difficult (if not impossible) when using the regular seeded catalyst method.

4.2.2.3 2D distribution of the NW density

In this part of the work, a possibility to control NW density by varying the position of the catalyst source with respect to the substrate was investigated. As described above, in an effort to establish the average distance and the mechanism of the vapor-phase transfer of the catalyst, a small seed-sample coated with a metal catalyst layer (a catalyst source) was placed upstream from the growth substrate. NWs of varying density grew across the surface of the growth substrate even when the substrate was positioned at a significant distance (e.g., more than 10 mm) away from the catalyst source.

Both the in situ catalyst deposition and the degree of the precursor supersaturation inside the catalyst during the VLS growth should depend on the temperature. Therefore, variations of the thermal conditions between the edges of small substrates and their middle regions were expected to introduce additional non-homogeneity of the NW density. To eliminate the contribution of this lack of homogeneity when investigating the two-dimensional distribution of the NW pattern with respect to the catalyst source, the NW density was analyzed after growing NWs across the entire 2-inch SiC substrate that is normally used as the wafer carrier.

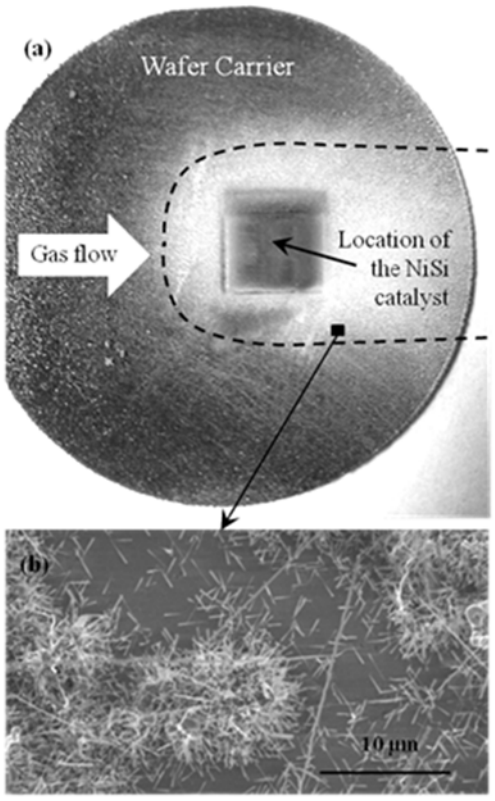

Figure 4.5 (a) A photograph of the wafer carrier after NW growth. One can see the location of a 1 x1 cm substrate covered with NiSi that was used as the catalyst source. The dotted line shows the approximate boundary of the NW region formed by the vapor-phase catalyst delivery—the white area surrounding the location of the catalyst. Both the diffusion through the boundary layer and the gas flow direction influence the macroscopic NW distribution. (b) A SEM image of the NWs growing on the wafer carrier due to the vapor-phase catalyst delivery mechanism.

Figure 4.5(a) shows the 2-inch 4H–SiC wafer carrier covered with dense NWs grown as a result of the vapor-phase transfer of the catalyst from the catalyst source. The milky (i.e., the white) regions correspond to higher NW density (as revealed by the magnified image in Figure 4.5 (b)). The dark square region in the middle of the wafer carrier shows the position of the catalyst source (a piece of a substrate covered with a layer of NiSi). It should be noted that the overall NW density on the surface of the wafer

carrier is much higher than that in Figure 4.4. This is because the surface of the wafer carrier had a polycrystalline layer of SiC before the NW growth, which created much higher density of preferential surface cites for the in situ catalyst deposition and NW growth. However, this surface was convenient for investigating the NW density variation with respect to the catalyst source.

The region of high NW density was found to be significantly extended along the gas flow direction downstream from the catalyst source (Figure 4.5 (a)). This indicated that the gas flow (i.e., the forced convection) is responsible for transferring the metal catalyst inside the hot zone over more than a few centimeters from the source. Naturally, the catalyst-carrying gas-phase species, which diffuse upward through the stagnant layer and reach the main gas stream, get picked up by the gas flow and transported over significant distances before aggregating into metal clusters at the growth surface contributing to the NW growth by the VLS mechanism.

However, high NW density was also found upstream from the source (Figure 4.5 (a)). Since it is known that a laminar flow is established inside the hot zone of this reactor, only gas- phase diffusion through the stagnant layer above the surface of the wafer carrier (i.e., the boundary layer) could be responsible for the catalyst transfer in the upstream direction from the source. Similar results were obtained when using Ni metal layer as a source of the catalyst for the vapor-phase delivery.

4.2.3 Role of poly-Si islands and the role of C/Si ratio

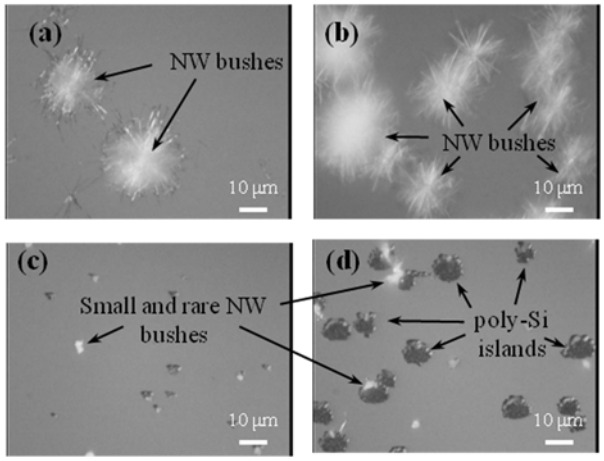

Figure 4.6 Growth of NW bushes rather than individual NWs, which happens at too low value of the C/Si ratio. (a) and (b) show optical micrographs of upstream and downstream locations of a substrate, with NW bushes grown by the vapor-phase catalyst delivery mechanism. (c) and (d) are for a similar substrate, however, with significantly reduced supply of the metal catalyst. Much smaller and more rare NW bushes in (c) and (d) reveal poly-Si islands serving as nucleation centers for the NW bushes in (a) and (b)

When the growth runs using the vapor-phase catalyst delivery approach were conducted outside of the optimized process window, this resulted in either formation of dense NWs over the entire surface or formation of bushes composed of randomly oriented NWs (Figure 4.6(a),(b)) that do not follow the epitaxial growth pattern reported in section 4.2.2.2 (Figure 4.4 (b), (c)). The density of the bushes was found to vary along the gas flow direction and was often increasing downstream (Figure 4.6 (a) and (b)). This suggested that nucleation of dense NWs or NW bushes may be influenced by factors other than the catalyst transfer from the source (which, as described above, normally causes higher density of nucleated NWs at the locations closer to the catalyst source). To investigate the bushes nucleation mechanism, a supply of the metal catalyst was

significantly reduced to suppress the NW growth and reveal possible nucleation centers that are otherwise hidden under the bushes.

Indeed, polycrystalline Si islands were observed at the growth conditions of reduced metal catalyst supply (Figure 4.6 (c) and (d)). The islands were similar to islands that were observed during the regular catalyst-free epitaxial growth conducted in the same reactor at similar growth conditions. The variation of the Si island density across the substrate matched the density of the NW bushes grown at identical growth conditions but with adequate supply of the metal catalyst (Figure 4.6 (a) and (b)]. An upstream location and a downstream location are shown in Figure 4.6in order to illustrate that the change in the density of the NW bushes from upstream to downstream correlates with the corresponding change in the size and density of the polycrystalline silicon islands.

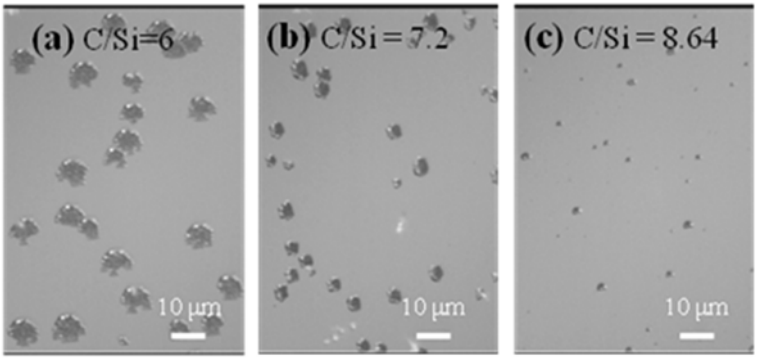

Figure 4.7 Optical micrograph of poly-Si islands visible thanks to the low supply of the metal catalyst. Three different values of the C/S ratio were used: (a) C/Si =6, (b) C/Si = 7.2, (c) C/Si = 8.64. High enough C/Si allows entirely avoiding poly-Si island formation.

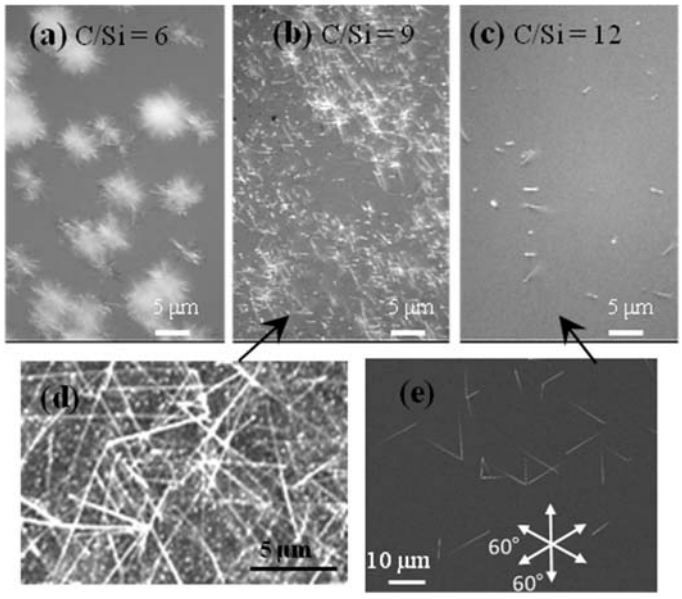

Figure 4.8 Transition from bushes of NWs at C/Si = 6 (a) to dense randomly oriented NWs at C/Si = 9 (b), and to the desirable individual NWs with substrate-determined orientations at C/Si = 12 (c). (d) and (e) show magnified SEM images for (b) and (c) respectively. This trend also correlates with the trend of poly-Si island reduction at higher C/Si ratio (Figure 4.7).

The role of the C/Si ratio in promoting (or suppressing) the undesirable formation of polycrystalline islands and, consequently, the NW bushes was investigated. It was established earlier that the density of poly-Si islands can be reduced by increasing the C/Si ratio[75]Again, a low catalyst supply was used to investigate poly-Si islands without masking them by the NW bushes. The density of the poly-Si islands was found to significantly decrease with increasing the C/Si ratio (Figure 4.7). Relatively big poly-Si islands that form at C/Si = 6 cause formation of NW bushes (Figure 4.8 (a)). At C/Si = 9, only very small poly-Si islands should form according to Figure 4.8(c), which results in growth of dense NWs without formation of big bushes (Figure 4.8(b)). Finally, at C/Si = 12 and above, no poly-Si islands form, which leads to the growth of rare individual NWs

aligned along specific crystallographic orientations with respect to the substrate (i.e., following the epitaxial growth mode) (Figure 4.8 (c)).

In summary, it was established that conditions of too low C/Si ratio favor undesirable nucleation of poly-Si islands, which in turn serve as nucleation centers for growth of NW bushes. It is logical to suggest that the rough surface of poly-Si islands serve as preferential sites for agglomeration of metal nanoclusters, which causes the high concentration of NWs forming the bushes.

4.2.4 Conclusion for the vapor-phase catalyst delivery study

Vapor-phase metal catalyst delivery mechanism has been demonstrated to be a viable technique for VLS growth of SiC NWs.

Both gas-phase diffusion of the catalyst through the stagnant layer above the surface of the substrate and the catalyst transport by the main flow of the carrier gas were shown to influence the catalyst delivery to the growth surface. This offers significant flexibility for selecting the geometry of the hot zone and a relative position of the catalyst source with respect to the substrate.

The vapor-phase catalyst delivery technique has an advantage of producing very low density of NWs (Figure 4.8(c)). This property of the vapor-phase metal catalyst delivery techniques along with its apparent ability to deliver catalyst to a complex substrate topology justified use of the new technique in this dissertation work for investigating growth of SiC NWs on different SiC crystallographic plains. The details of this effort are reported in the next section.

4.3 Growth on different surfaces

Portions of the following section is reprinted with the permission from Thirumalai, R. V. K. G., Krishnan, B., Levin, I., Davydov, A. V., Sundaresan, S. G., Merrett, J. N., & Koshka, Y. (2012). Growth of SiC Nanowires on Different Planes of 4H-SiC Substrates. *Materials Science Forum*, *717-720*, 1279–1282. doi:10.4028/www.scientific.net/MSF.717-720.1279

4.3.1 Choice of the catalyst formation method

Based on the previous experiments, the vapor-phase catalyst delivery technique was employed as a novel approach to investigating the influence of a SiC substrate on crystalline structure (e.g., the polytype) and orientation of SiC NWs and growing SiC NWs on the different planes of SiC mesas. The experiments were conducted in the same hot-wall CVD reactor and the same growth conditions. This section summarizes the advantages of the vapor-phase catalyst delivery technique compared to the traditional seeded catalyst method [32].

4.3.1.1 Growth by seeded catalyst method (blanket deposition of metal)

Dense and randomly oriented NWs were grown when pieces of commercial heavily doped n-type 4H-SiC (0001) wafers were used as the growth substrates, with Au[70], [72], Ni or NiSi catalyst layers blanket deposited on the samples by physical vapor deposition. This dense growth did not allow identification of the NW orientation. More importantly, it is unlikely that epitaxial relationship between the NW and the substrate was realized under the condition of dense NWs interfering with each other during their growth. To identify factors affecting NW density, various changes in growth

conditions were implemented. The NW density was found to be sensitive to the thickness of the catalyst layer and pre-growth heat-treatment conditions in addition to the growth conditions. The use of the NiSi catalyst at the same growth temperature of 1150°C yielded significantly lower densities of NW per unit area of the substrate compare to the Ni assisted growth..

4.3.1.2 Advantage of vapor phase catalyst delivery

Since the catalyst is delivered in a vapor form, it can facilitate NW growth in intricate sections of the substrate with complex topology. For example, it may be difficult to coat mesa sidewalls evenly with a metal catalyst layer. In contrast, growth on mesa sidewalls can be easily achieved by using vapor-phase catalyst delivery technique. In addition, vapor-phase catalyst delivery technique can produce very low and controllable density of NWs (Figure 4.8(c)). These advantages have been exploited in this work to study orientations of the SiC NWs grown on different SiC crystallographic plains and investigating polytype relationship between growing NW and a SiC substrate.

4.3.2 Growth on (0001) plane of a SiC substrate

Portions of the following chapter are reprinted with the permission from Krishnan, B., Thirumalai, R. V. K. G., Koshka, Y., Sundaresan, S., Levin, I., Davydov, A. V, & Merrett, J. N. (2011). Substrate-Dependent Orientation and Polytype Control in SiC Nanowires Grown on 4H-SiC Substrates. *Crystal Growth & Design*, *11*(2), 538–541. doi:10.1021/cg101405u

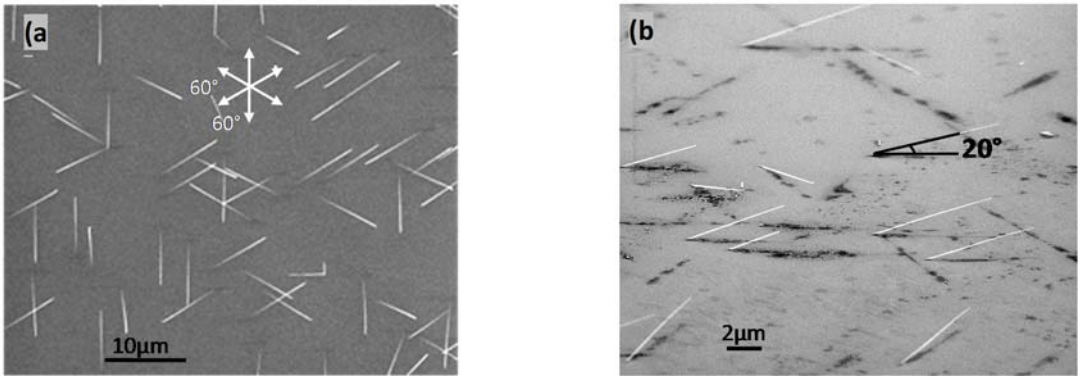

Figure 4.9 SEM images of (a) the top and (b) a tilted views of sparse NWs grown using NiSi catalyst at 1150°C

Growth using vapor-phase catalyst transfer of a metal catalyst from a NiSi source to an unpatterned (0001) top surface of 4H-SiC substrate resulted in sufficiently rare SiC NWs, which could have not been achieved when using the traditional seeded catalyst method. NWs grew along six directions (Figure 4.9). They all formed 20° angle with the c plane of the substrate (Figure 4.9 (b)), and their projections on the c plane corresponded to one of the six equivalent $\langle 10\bar{1}0 \rangle$ crystallographic directions (i.e., the projections were aligned at 60° with respect to each other) (Figure 4.9 (a)). It should be noted that the 20° is the angle with respect to the basal plane of the substrate rather than the substrate surface that was off-axis with respect to the c plane in most of the substrates used. The angle was calculated from the angle between the NW axis and the surface by accounting for the surface off-axis angle. The same 20° angle to the c plane was observed for all six NW axis directions.

Based on the experience of other semiconductor materials, the vertical NW orientation was also expected to be energetically favorable. Unfortunately, when vapor

phase catalyst delivery method was used to obtained low NW density, no vertical NWs were visible.

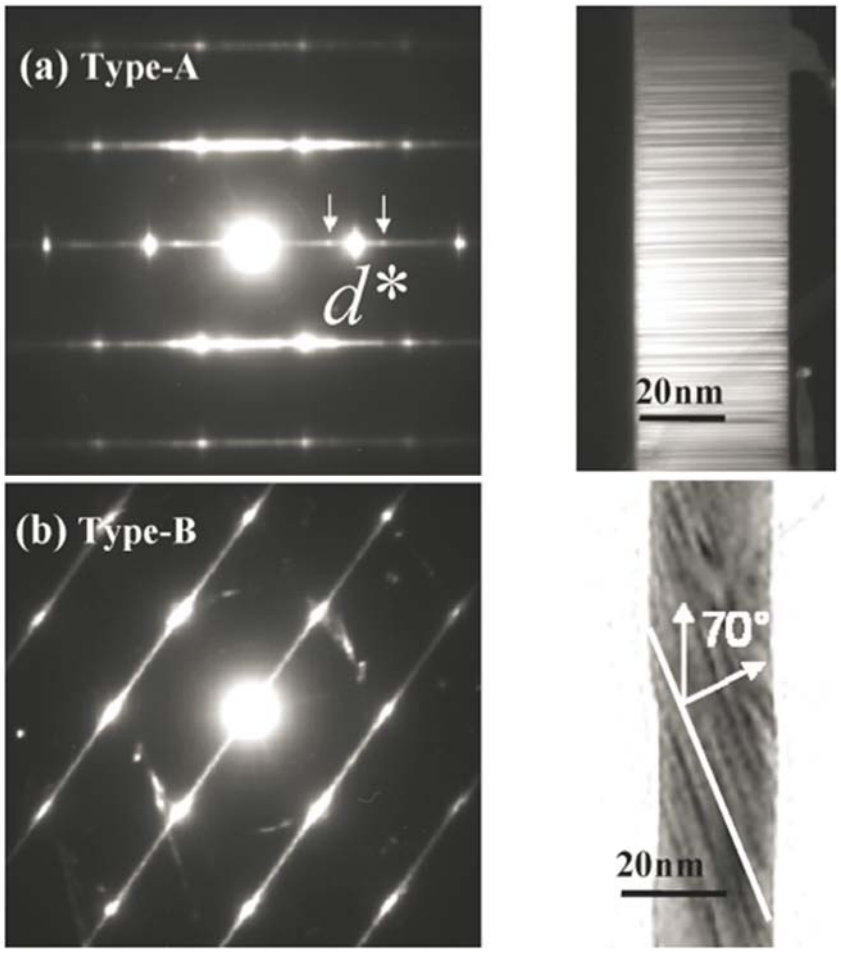

Figure 4.10 SAED of (a) Type-A NW having the fault planes orthogonal to the NW axis and (b) Type-B NW with the growth axis at 70^0 to the [0001] direction of the substrate. SAED in (a) reveals the 4H polytype with a strong stacking disorder as manifested in superlattice reflections at 1/4d* indicated with arrows. SAED in (b) displays a 3C NW with a high density of {111} SF

Growth using seeded catalyst method (blanket deposition of the Ni catalyst on the growth substrate) was also investigated. A certain fraction of nearly vertical NWs was

achieved. Selected area electron diffraction (SAED) patterns and bright/dark field images were collected for the NWs from the Ni-based sample. Two main types of NWs were observed (Figure 4.10), which hereafter will be referred to as Type A and Type B. Both types exhibit high densities of stacking faults (SF) as reflected in the nearly continuous rods of diffuse intensity in the SAED patterns. In Type A, the faults planes are orthogonal to the NW axis and the electron diffraction (ED) patterns exhibit discernible maxima at 1/4d* indicated using arrows in Figure 4.10 (a), where d* is a reciprocal of the c-layer spacing for hexagonal SiC. These results confirmed the presence of the 4H polytype (even though with a strong stacking disorder) consistent with the XRD patterns reported in the previous work [121]. The NW axis in Type A was parallel to the [0001] direction.

In contrast, the SF planes in Type B were aligned at 70^0 with respect to the NW axis (Figure 4.10 (b)). According to the SAED (Figure 4.10 (b)), these NWs exhibited the 3C polytype, with the NW axis parallel to the [111] direction. It should be noted that the Type-B alignment of SFs was dominating also in other samples investigated in this dissertation work, including the samples produced with NiSi and Au catalysts.

While it was expected that the catalyst composition and growth temperature should also influence the growth direction of the NWs, no such effect was observed in this study.

4.3.3 Growth on crystallographic planes other than (0001)

Portions of the following chapter are reprinted with the permission from R. V. K. G. Thirumalai, B. Krishnan, A. V. Davydov, J. N. Merrett and Y. Koshka, “Growth on differently-oriented sidewalls of SiC mesas as a way of achieving well-aligned SiC nanowires,” Cryst. Growth & Design, 2012, 12, 2221−2225

4.3.3.1 NW axes orientations and NW alignment

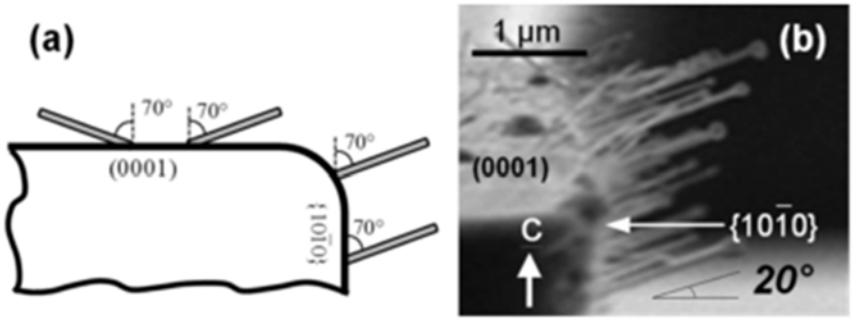

Figure 4.11 A side view demonstrating the growth angle of the NWs with respect to the c-axis: (a) a growth schematics, (b) an SEM image of NWs growing on the vertical sidewalls of a SiC mesa, confirming the 70° angle with respect to the c-axis (20° angle with respect to the basal plane).

Rectangular and circular 4H-SiC mesas of varying dimensions were used to study NW growth on planes other than (0001). A possibility to obtain well-aligned SiC NWs by choosing proper crystallographic orientations of the growth surface was explored. The mesas were formed by RIE on the top (0001) surface of a 4H–SiC substrate. The process steps involved in forming these mesas are described in the experimental section 3.1.2.3.

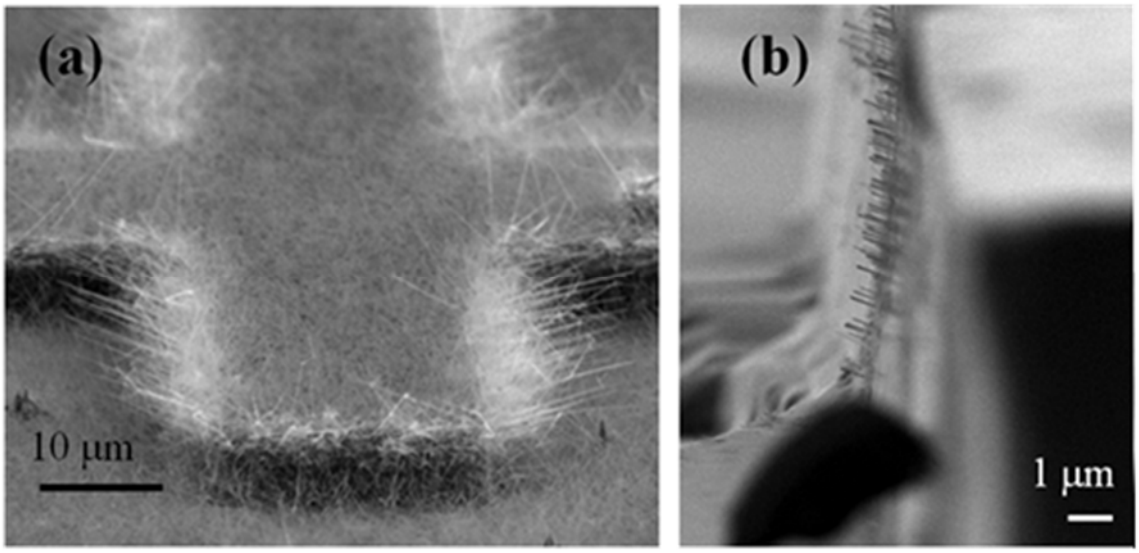

Figure 4.12 Use of the vapor-phase catalyst delivery to grow on patterned surfaces: (a) dense NWs growth on the vertical mesa walls and the horizontal surfaces with significant RIE damage at high catalyst supply, (b) Rare NW growth at very low catalyst supply in combination with H_2 pre-etching of the mesa surface causing rare spots of NW nucleation only at defects (e.g., scratches) on the vertical sidewalls.

When vapor phase catalyst delivery method was used, NWs successfully grew on all available surfaces of 4H–SiC mesas. Initially, very dense NWs were achieved on the vertical sidewalls [Figure 4.12 (a)], and their density could not be significantly reduced by merely reducing the amount of the catalyst source available for the vapor-phase catalyst delivery.

It was speculated that the dense random NW growth was a result of surface damage at the vertical sidewalls, which promoted heterogeneous nucleation of the metal catalyst and enhanced formation of a high-density metal clusters for VLS NW growth. To reduce the lattice damage caused by RIE, the NW growth experiments were repeated on mesas that were etched in H_2 flow at 1500 °C for 10 min before the NW growth. The NW

growth was conducted without any catalyst source placed inside the hot zone, but instead, it relied exclusively on the catalyst memory effect caused by the contamination of the hot zone with the catalyst during the previous runs.

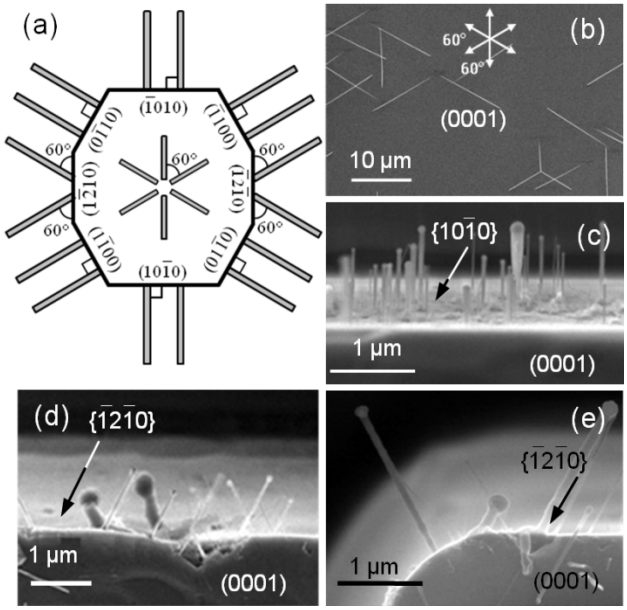

Figure 4.13 A top view of SiC NWs growing on the top surface and the vertical sidewalls of SiC mesas: (a) a schematics showing azimuth orientation of the growth direction, (b) an SEM image of NWs growing on (0001) surface, (c) and (d) NWs growing on {10-10} and {-12-10} planes respectively. (e) shows simultaneously NWs growing on (0001) surface, a {-12-10} plane and on the rounded edge of the mesa representing a gradual transition from {-12-10} to {10-10}.

Because of the minimized catalyst supply and significantly reduced surface roughness, the NW density was drastically reduced on most of the mesa surfaces. Figure 4.13(a) shows schematic projection of NW orientations onto the substrate's (0001) plane, which was observed experimentally in Figure 4.13(b)-(e). Similar to the results of the growth on unpatterned (0001) 4H-SiC surfaces (section 4.3.2), the NWs on the top

(0001) surfaces of the SiC mesas were found to grow along six directions (Figure 4.13 (a) and (b)). As described in section 4.3.2, they all formed 20° angle with respect to the c-plane of the substrate, and their projections on the c-plane corresponded to one of the six equivalent <10-10> crystallographic directions (i.e., the projections are aligned at 60° with respect to each other).

Only these same six orientations of the NW axes were observed when growing on vertical mesa sidewalls having a wide range of crystallographic orientations, which were provided by circular mesas and the rounded edges of the rectangular mesas.

The top-down SEM view was used for evaluating the angle of the NW projections on the c-plane. The use of any particular {10-10} mesa sidewall plane resulted in only one corresponding NW orientation, wherein the NW projection on the c-axis was perpendicular to the corresponding {10-10} plane (Figure 4.13 (a) and (c)).

Two different NW orientations often coexisted when growing on any particular {-12-10} mesa sidewall. Projection of any of those NWs on the c-plane still corresponded to one of the six orientations observed when growing on the top (0001) surface as discussed above (Figure 4.13 (a) and (d)). Furthermore, mesa sidewalls corresponding to a transition from {10-10} to {-12-10} crystallographic planes still exhibited a maximum of two NW orientations (see for example the rounded mesa edge in Figure 4.13 (e).

However, it was established that the NWs on {10-10} mesa sidewall planes were not perpendicular to the corresponding planes. In fact, all NWs formed 70° angle with the c-axis (i.e., 20° angle with the c-plane), which is the same angle as that of the NWs growing on the (0001) surface (Figure 4.13). Only this angle with respect to the c-plane could be observed when growing on any other vertical sidewall plane as well as on any of

the rounded mesa edges or the rounded edges of the SiC substrates (Figure 4.14). Those rounded edges represented all possible planes when observing a transition from (0001) top surface to the vertical sidewall planes Furthermore, growth on the rounded edges corresponding to the transition from (0001) plane to the {10-10} vertical sidewalls resulted in a single orientation of the NW axes (Figure 4.14, thereby providing only well-aligned parallel NWs grown in the particular location.

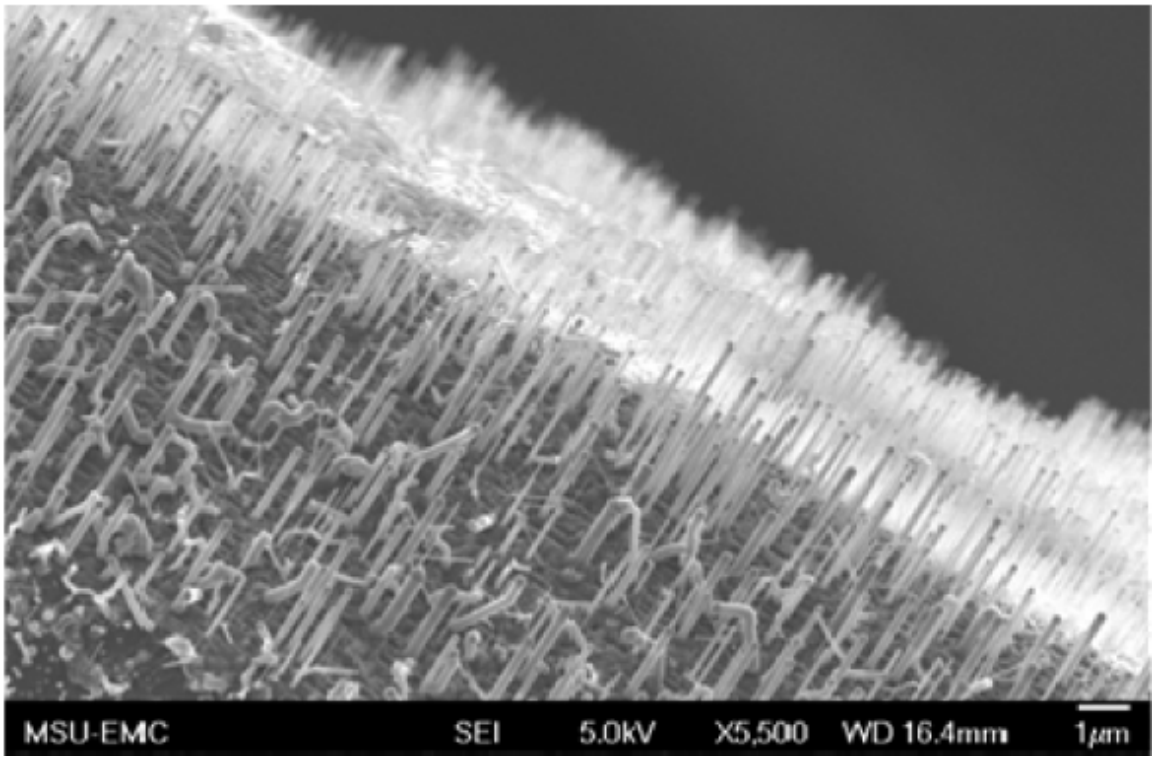

Figure 4.14 Aligned SiC NWs growing on the {10-10} plane of the SiC substrate and across the rounded edge corresponding to the transition from (0001) substrate surface to the {10-10} plane

Besides individual rare NWs (Figs. 4.10 and 4.14), selected locations of the vertical sidewalls exhibited relatively dense NW arrays [Figure 4.12 (b)]. In all the cases,

those arrays corresponded to a surface damage. This result confirmed the conclusion made in section 4.2.3 that surface roughness is essential for promoting clustering of the metal catalyst at higher concentrations and therefore should be avoided.

An observation from Figure 4.14 is the presence of metal droplets at the tip of the NWs, which are difficult to detect for the normally thin NWs but are clearly distinguishable for more rare thick NWs. This confirmed that the vapor-phase catalyst delivery of the catalyst indeed takes place, causing the NWs grow by the VLS growth mechanism.

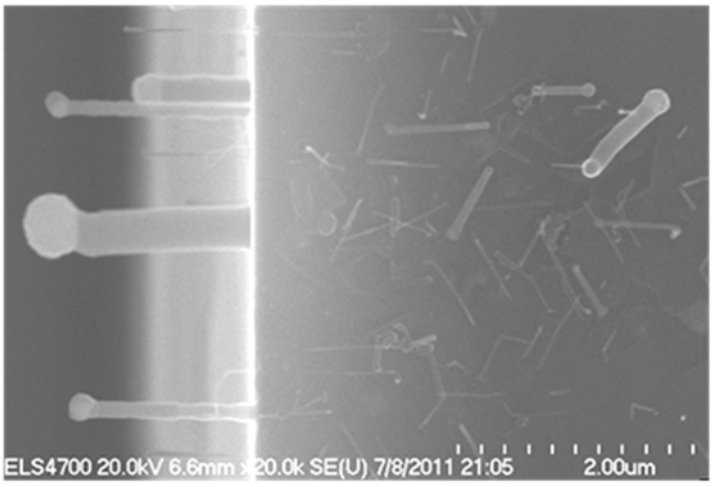

Figure 4.15 A mesa samples with a few thicker NWs formed by vapor-phase catalyst delivery, which allows detecting the catalyst drop at the tip of the NWs

4.3.3.2 NW polytype control.

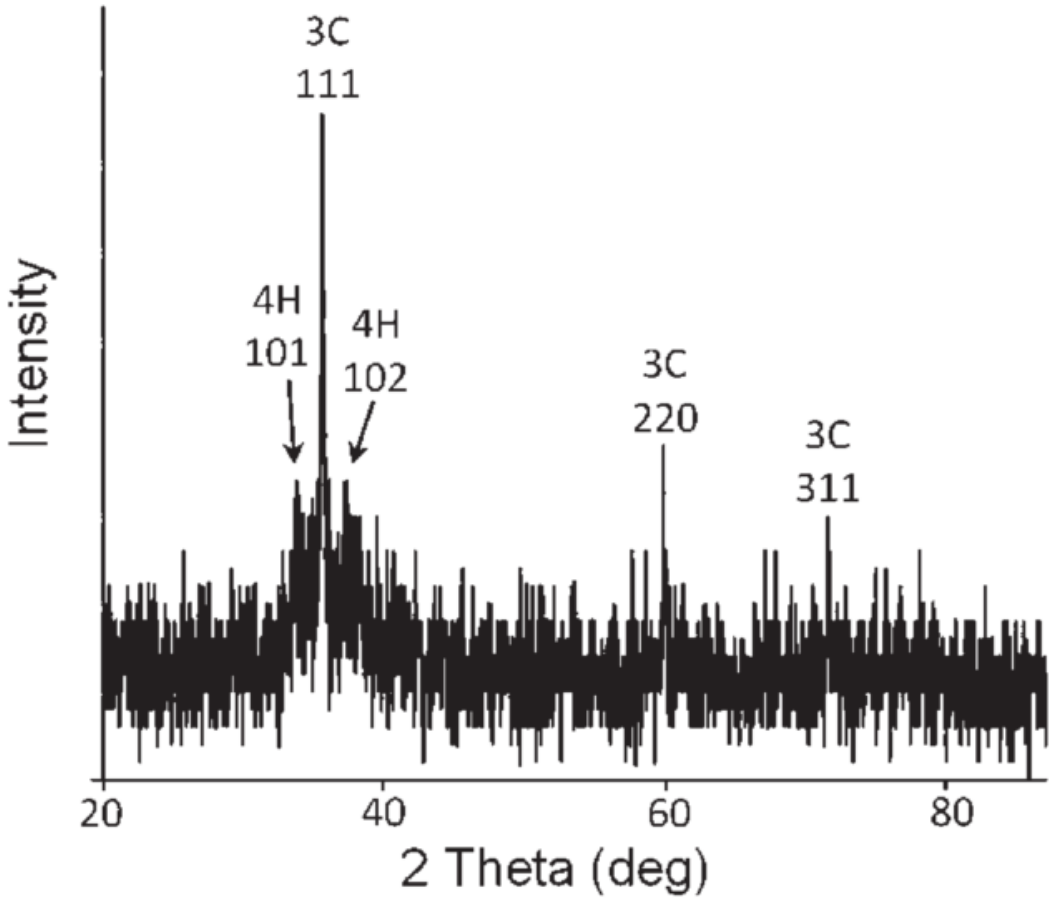

Figure 4.16 XRD pattern from dense SiC NWs grown on 4H-SiC substrate at 1150°C [32].

Next, polytype investigation was conducted. XRD (Figure 4.16) and high-resolution TEM measurements on samples with sufficiently high density of the NWs, and high-resolution TEM measurements showed domination of 3C NWs with their growth axis corresponding to the <111> direction. Since those techniques did not allow us to reliably establish if the characterization data correspond to the NWs grown on the top surface or the vertical sidewalls of the mesas, EBSD measurements targeting individual

NWs grown on the vertical sidewall (Figure 4.17) were used to supplement the XRD and TEM results. For statistical validity, EBSD patterns from multiple NWs that grew on the mesa top surfaces and on sidewalls were analyzed using crystallographic data for most common SiC polytypes, including 3C, 2H, 4H, and 6H.

Only 3C phase indexing produced a consistent and accurate match to the experimental diffraction results. Figure 4.17 (b) shows an example of 3C indexing of EBSD from a NW that grew on the (10-10) sidewall. However, since NWs grew at various angles with respect to both the top and the side substrate facets and, therefore, their absolute orientation in the EBSD geometry setup was not unequivocal, it was difficult to reliably determine their growth axis. The results of TEM study of random 3C-SiC NWs in section 4.3.2 showed the growth axis to be ⟨111⟩. Therefore, by using the combination of the TEM and the EBSD results, it was concluded that all 3C-SiC NWs that grew along one of the six directions with respect to the substrate had their growth axes along the ⟨111⟩ crystallographic direction.

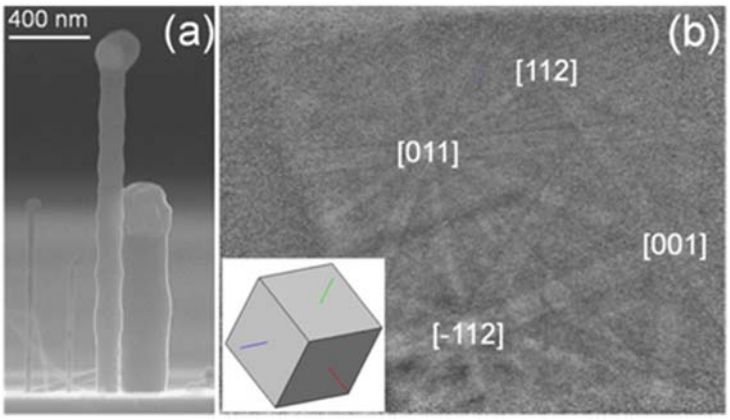

Figure 4.17 (a) SEM of 3C-SiC NWs growing on $\{10\bar{1}0\}$ surface and (b) corresponding EBSD pattern with simulated crystallographic orientation of the 3C unit cell in the inset.

4.3.4 Discussion

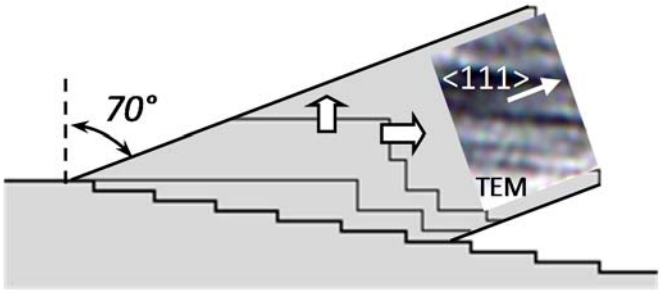

Figure 4.18 Diagram of the NW growth at 70° with respect to the c-axis of the substrate. The inset shows the TEM image of a 3C NW with SF parallel to the basal plane of the substrate.

As discussed in section 4.3.2, when 3C NWs with [111] axis grew at 70° angle with respect to the c axis, this resulted in the {-111} plane (which is also the plane for the SF in the 3C-SiC NWs) being parallel to the basal plane of the substrate (Figure 4.18). In addition, since the NW projection on the (0001) plane points along one of the six equivalent ⟨10-10⟩ crystallographic directions, it is unambiguous that the {112} and {110} planes in 3C NWs are parallel to the {10-10} and {11-20} planes of the 4H substrate, respectively. It is suggested that this orientation relationship yields the best lattice match between 3C NWs and the 4H (0001) substrate. This result agrees with the epitaxial relationship between the 3C-SiC inclusions and the 4H-SiC matrix and between the 3C films and the hexagonal SiC surfaces used for the 3C heteroepitaxial growth. Also, as illustrated by schematic atomic alignment in Figure 4.19, it provides a very small in-plane lattice mismatch of 0.2% between 3C- and 4H-SiC. Noteworthy, this lattice

alignment is the same as for the epitaxial growth of hexagonal ⟨0001⟩ oriented GaN NWs on a cubic Si (111) substrate. [110]

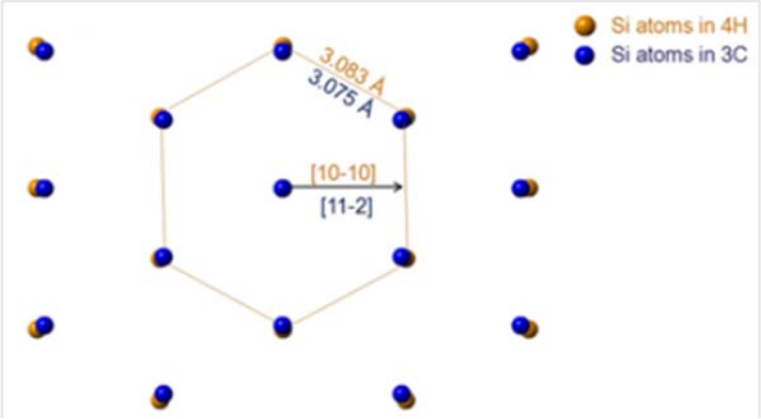

Figure 4.19 Atomic arrangement of 3C (111) plane on 4H (0001) plane with the following epitaxial relationships: (111) 3C‖(0001) 4H and $[11\bar{2}]3C\|[10\bar{1}0]$ 4H. Note that a very small in-plane lattice mismatch of 0.2% was calculated using 3C and 4H lattice parameters.

While as many as six different orientations of the NW axes (i.e., six equivalent <10-10> crystallographic directions with respect to the substrate lattice) are possible when growing on the (0001) surface, growth on {10-10} surfaces as well as on the surfaces that are transitional from (0001) to {10-10} provides only a single orientation of the 3C-SiC NWs for the particular growth surface (Figure 4.14).

When using commercial (0001) 4H-SiC substrates, the {10-10} surface planes are provided by some of the vertical sidewalls of the mesas formed on the top substrate surface. This enables the growth of well-aligned close-to-horizontal NW arrays (more precisely, 20° inclined with respect to the substrate surface ignoring possible off-cut

angle) (Figure 4.14), which is convenient for device fabrication using conventional planar lithography.

4.4 Attempts to characterize the electrical properties

4.4.1 Metal contacts formation using conventional photolithography

In order to investigate electrical properties of the grown NWs, several approaches were examined. A standard approach to forming metal contacts without using e-beam lithography (which is absent at MSU or our collaborators) has been attempted. The basic flow of steps towards forming metal contacts using regular optical lithography is as follows:

1. Deposit the 1st metal layer and define the electrode pattern using conventional photolithography;
2. Harvest SiC NWs from the growth substrate. It was done by ultrasonic treatment of the sample in a solvent solution;
3. Disperse a drop of the NW solution onto the dielectric substrate. The substrate was a Si wafer covered with a thermally grown SiO2 layer. Use of the AC electric field during NW dispersion from the solution (di-electrophoresis) was investigated to achieve NWs better aligned between the give pair of electrodes. The di-electrophoresis approach was developed, however it remains to be optimized to achieve any improvement in the NW alignment.
4. Let the solution dry, in order to deposit NWs on the dielectric surface. Some fraction of the NWs should end up located between some pairs of the electrodes.

5. Deposit and pattern the 2nd (top) layer of the metal electrodes. The metal is selected thick enough to be used with a probe stand or wire-bonder. The two ends of the NW are sandwiched between the 1st and the 2nd metal layer.
6. Form the bottom Ohmic contact.

Figure 4.20 shows the pattern of photolithography masked that was designed to fabricate the 2nd metal layer (the top layer). The 1st - layer mask (not shown) included only large square regions (contact pads), having slightly smaller dimensions to provide some margin for the alignment error, while omitting the small features serving as 4-point-probe contacts.

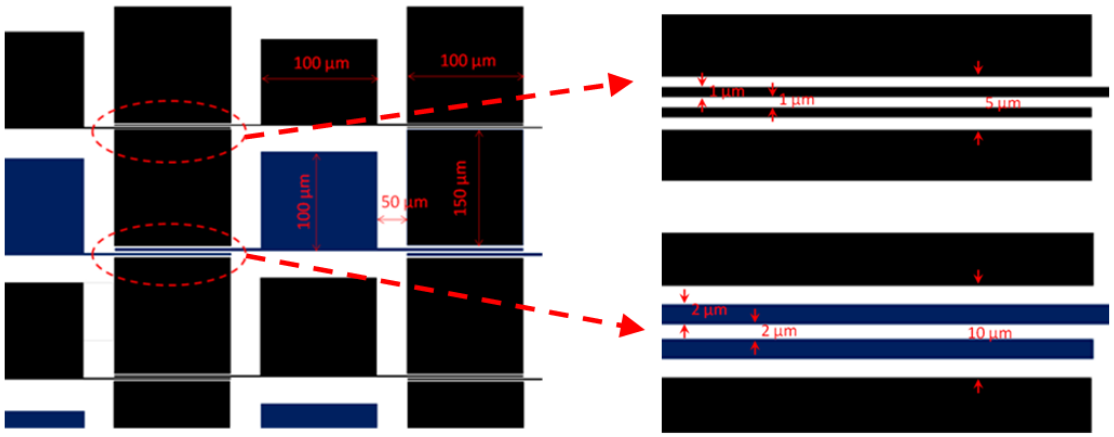

Figure 4.20 The photolithography mask designed to provide 4-point contacts for SiC NWs deposited from the solution and aligned using a di-electrophoresis. The figure to the right shows a magnified view. Two different spacings and widths of the metal contacts were provided.

Metal deposition and patterning of the first-layer contacts using the first mask was conducted. The pattern was used for di-electrophoresis deposition of the NWs where

electric field applied to the NW through the solvent aligned the NW with the contacts where electric field is applied. It was observed that only small number of NWs end up having desirable alignment. The use of di-electrophoresis is yet to bring desirable results. Furthermore, the density of the NWs in the solution should be controlled to avoid deposition of multiple NWs at the same pair of contacts. This approach appears to be difficult to use for our NWs without e-beam lithography. However, being a conventional approach applied to NWs of other semiconductor materials, it is suggested as a subject of the future work. In this dissertation instead, formation of metal contact to individual SiC NWs using FIB metal deposition was selected as more promising.

4.4.1.2 Metal contacts formation using focused ion beam

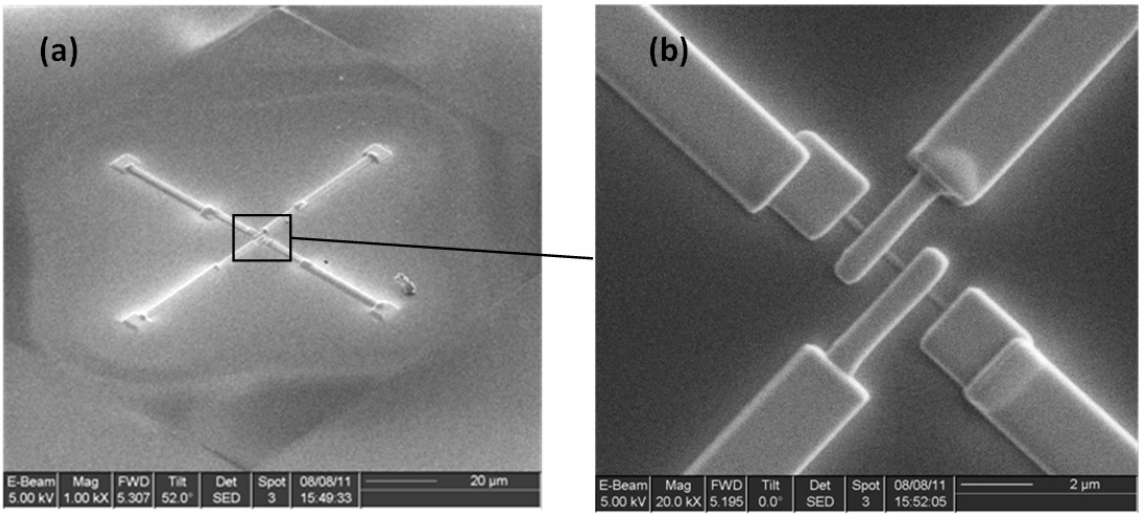

Figure 4.21 SEM images of the metal contacts to an individual SiC NW for the four-point-probe measurements of the NW conductivity: (a) the full view and (b) the magnified view. The contacts were made by the focused ion beam (FIB) direct-write technique.

Focused ion beam (FIB) was used for depositing very small metal contacts on SiC NWs. This technique is especially beneficial when NW density is very low. A 4-point-probe pattern was designed, and Pt deposition with an FIB instrument at AFRL was used. The pattern dimensions were designed to ensure reasonable deposition time. The pattern did not include contact pads, which were to be fabricated later using a conventional photolithography.

The process involved in this attempt can be briefly described as follows. SiC NWs were first harvested from the growth substrate. An individual NW of sufficient length (4-5 μm) was then found by scanning the surface of the substrate under SEM. FIB was used later used to deposit a thin layer of Pt on the nanowire to form a 4-point probe pattern. Figure 4.21 (a) and (b) show the panoramic view and the magnified image of four contacts to an individual SiC NW. The contact width and the contact spacing were roughly 0.5 μm.

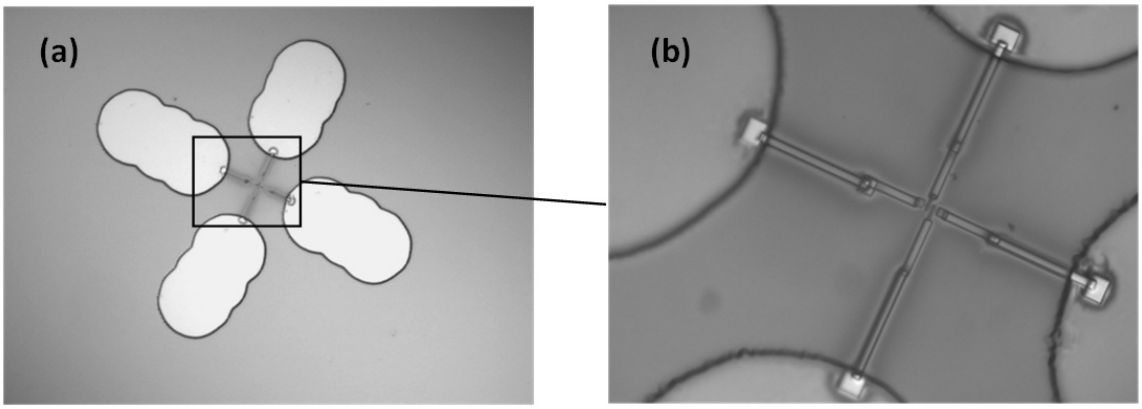

Figure 4.22 Optical micrographs of the SiC NW test structure with large contact pads fabricated by the conventional photolithography: (a) the full view and (b) the magnified view. The images were taken after the photoresist development prior to the metal deposition. The pattern was created by a sequential exposure of the neighboring areas of the photoresist using a single circular feature of the photolithography mask.

As explained earlier FIB is a very slow process, it would be time consuming to form contact pads big enough for wire bonding. Sufficiently large metal pads suitable for the probe stand or wire bonding were fabricated by a conventional lithography (Figure 4.22). Photoresist at the desirable region of the sample (contacting the end of one of the metal contact lines) was exposed through the selected circular windows. (Figure 4.22 Figure 4.20 (a) and (b)). The metal contact fabrication in the first set of the experiments (Figure 4.22) was done by lift-off using 200Å Ni/5500 Å Al layer. In the second set of the experiments, 300Å Ti/5000 Å Au contacts were formed, and wet etching was used instead of lift-off.

4.4.2 Conductivity Measurement

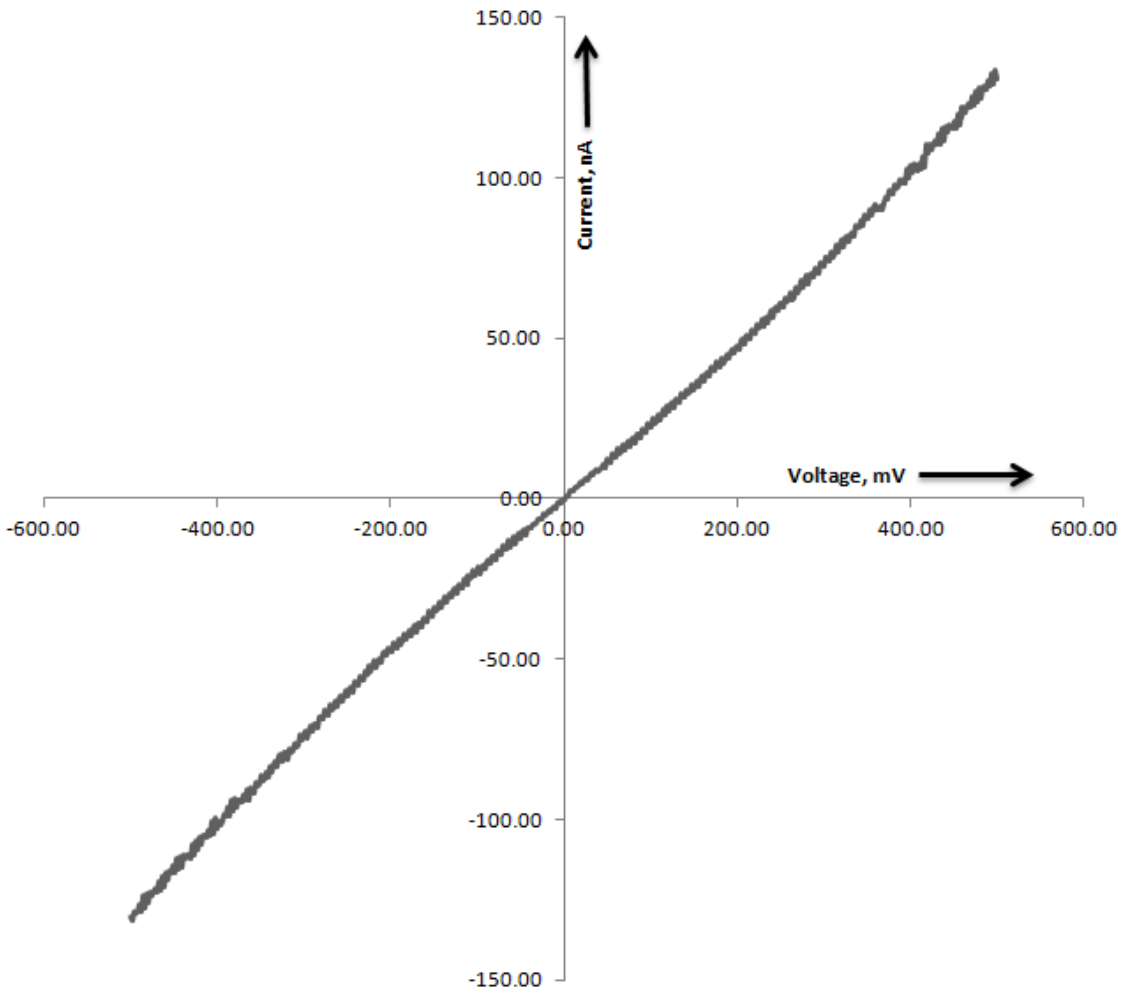

Figure 4.23 IV curve of a SiC NW using simple 2-point contact

The I-V characteristic for one pair of the fabricated contacts is shown in Figure 4.23. As expected, the characteristics is not ideally Ohmic. It is well-known that non-annealed metal contacts to SiC should normally exhibit a Schottky behavior [76]. Only for heavily doped samples (e.g., with the dopant concentration above 10^{20} cm^{-3} (see for example Ref. [77]) or high lattice defect concentration could a nearly Ohmic behavior be

expected due to the free carrier tunneling through the thin Schottky barrier or due to defect-related reverse-bias leakage current. The deviation from the ideal Ohmic behavior in the I-V characteristics of Figure 4.23 is consistent with the doping in a range significantly below 10^{20} cm^{-3}, although any more precise identification requires measurement for the NW resistivity.

While the fabricated test structure was designed specifically for enabling four-point-probe measurements to separate the contribution of the contact resistance (R_C), the four-point-probe measurements failed in both of the samples (i.e., two different fabrication processes). The contacts failed after initial measurements before they could be used in the four-point-probe configuration. The analysis of the failure is reported later in this section.

Only rough estimations of the NW conductivity are possible from the two-point-probe I-V characteristics. For a given pair of electrodes having 1um spacing, the total resistance between (R_{tot}), measured as the inverse of the zero-bias slope of the I-V dependence, was equal to ~5 MΩ. In order to evaluate extreme values of the NW conductivity that are consistent with the observed R_{tot}, the following considerations were used.

At first, R_C was assumed to be close to zero (which is of course unrealistic, especially in the non-annealed samples). For the given spacing between the two contacts of 2 um and the NW diameter of 280 nm, assuming electron conductivity and using the typical value of the free electron mobility of 380 $cm^2V^{-1}s^{-1}$ (while ignoring the impossible to evaluate carrier scattering by stacking faults in 3C-SiC), the net free carrier concentration would have to be just under 10^{15} cm^{-3}. This low value is in the range of

what is considered a difficult to achieve purity for SiC materials. However it is way too low to ensure the values of R_C even in the kΩ range, which could be expected in reasonable quality contacts of this size after annealing. And it is definitely too low to satisfy the assumption of the close-to-zero R_C, especially in our non-annealed samples. However, it is unknown if the presence of stacking faults could cause low R_C in the particular NWs investigated in this work. Therefore, the experimentally achievable in SiC doping close to $10^{15}cm^{-3}$ can be taken as a very rough estimate of the lowest possible value of the NW doping satisfying the I-V data.

If one makes a logical speculation that a much higher portion of R_{tot} is caused by R_C, this would mean higher values of NW conductivity (i.e., doping). Since R_C is unknown and could in principle have any value up to the R_{tot} (especially in the unannealed samples), the value of doping up to the very solubility limit (which is different in n-type and p-type and must depend on the crystalline structure in the material with so many SFs) is possible from this consideration.

The problem with that estimation of the highest possible value of doping is that doping close to the solubility limit would normally ensure much better (i.e., lower) than the given assumption R_C for most of the metal contact materials. However, there is no knowledge about the quality of the Pt contacts deposited by FIB, which means that poor (i.e., high) R_C could not be excluded as a possibility even when very high NW doping is used. Therefore, doping as high as the solubility limit is not inconsistent with the observed R_{tot}.

Unfortunately, all this means that considerations based on the presented two-point-probe I-V characteristics are unreliable for estimating the high limited of the NW conductivity.

4.4.3 Investigation of the failure of the FIB contacts

cc 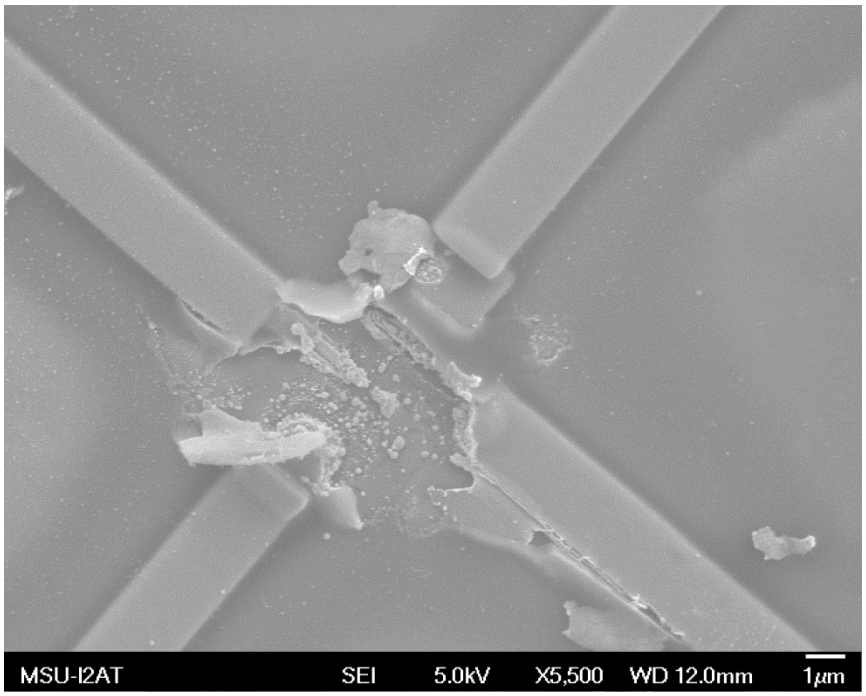

Figure 4.24 FIB contacts to NW after contact failure

It was concluded it this work that a mechanical damage of the NW contacts during the fabrication process by two different methods was very unlikely. Also, the contacts worked at the beginning of the electrical testing and failed only after a certain time. Contact damage as a result of electrical measurements was assumed. The reasons for failure at what appears to be a relatively low current density (122 A/cm^2) were investigated.

An SEM image of a NW with four contacts formed by FIB prior to the contact pad formation, packaging and electrical measurements is shown in Figure 4.21. In this sample, the lift-off procedure was used to form the Ni/Al contact pads. The same NW test structure after the electrical failure of the contacts (section 4.4.2) is shown in Figure 4.24. Another NW test structure with the contact pads formed by wet etching of the Ti/Au instead of the lift-off Figure 4.25. This figure was also obtained after the electrical failure.

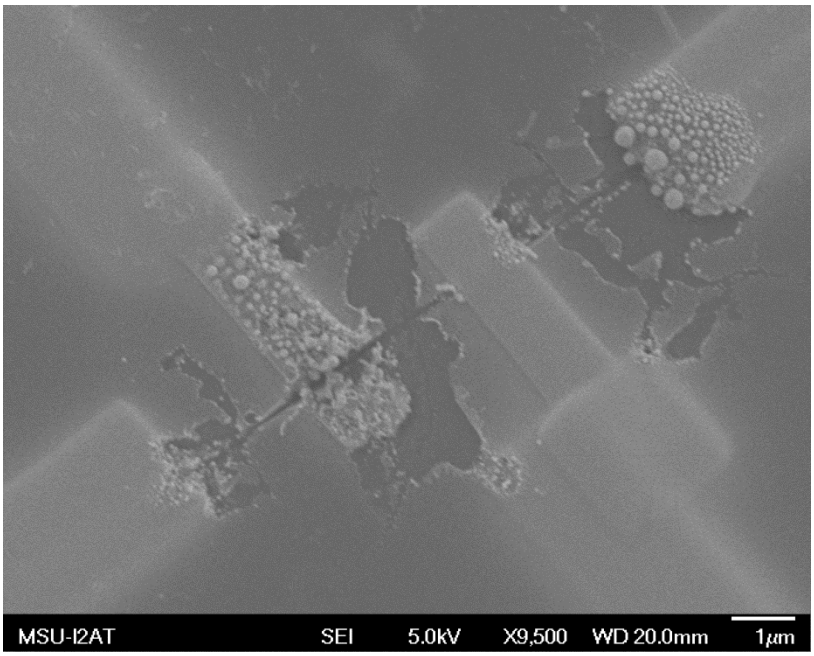

Figure 4.25 FIB contact second attempt formed by using wet-etching after contact failure

It is obvious that the Pt electrodes degraded in the regions of the contact. It is clear from Figure 4.25that the Pt degradation is particularly severe at the regions of the electrodes contacting or surrounding the NW. Considering the relatively low current

density, it is concluded that the quality of the Pt material deposited by FIB using two different instruments at two different research institutions is insufficient for this kind of electrical measurements.

CHAPTER V

SUMMARY AND CONCLUSION

5.1 New technique for controllable NW growth

The main results of this part of work are:

1. A method based on the vapor-phase metal catalyst delivery mechanism has been developed, which is a viable technique for VLS growth of SiC NWs. The catalyst can be easily delivered to differently oriented surfaces of a complex substrate topology, as was illustrated by growth on vertical sidewalls of SiC mesas.
2. The main growth trends and process dependencies for the new growth method have been established, including the factors influencing the NW density and formation of NW bushes.
3. A capability of achieving both very low and high NW density by controlling the C/Si ratio, substrate surface preparation, positioning of the catalyst source with respect to the substrate, etc were demonstrated.

These advantages of the new method can be utilized by others to move SiC NW research to the next level and explore NW-based device structures.

5.2 NW growth and characterization.

The three main results of the substrate-dependent growth of SiC NWs are:

1. A demonstration that the growth of 3C-SiC NWs on different surfaces of 4H-SiC substrates by CVD is governed by the epitaxial growth mechanism where (111) plane of the NWs plane is parallel to the (0001) plane of the substrate and the (112) NW plane is parallel to the (10-10) plane of the substrate, and
2. Development of a method for fabricating arrays of well-aligned (i.e., all-parallel) 3C-SiC NWs by the bottom-up approach, which is accomplished by epitaxial growth on crystallographically selected growth surfaces.
3. Evidences for the presence of 4H-SiC polytype, which offers a promise of a homoepitaxial growth of NWs reproducing the polytype of the substrate.

While as many as six different orientations of the NW axes (i.e., six equivalent <10-10> crystallographic directions with respect to the substrate lattice) are possible when growing 3C-SiC NWs on the (0001) surface, growth on {10-10} surfaces as well as on the surfaces that are transitional from (0001) to {10-10} provides only a single orientation of the 3C-SiC NWs for the particular growth surface.

When using commercial (0001) 4H-SiC substrates, the {10-10} surface planes can be provided by some of the vertical sidewalls of the mesas formed on the top substrate surface. This enables the growth of well-aligned close-to-horizontal NW arrays (more precisely, 20° inclined with respect to the substrate surface ignoring possible off-cut angle), which is convenient for device fabrication using conventional planar lithography.

5.3 Fabrication of SiC NW electrical test structures and electrical properties

The grown NWs have been characterized by multiple techniques including SEM, TEM, XRD and EBSD for identification of the material and its polytype. However, for use in devices and sensors, establishing electrical properties of the grown NWs is important. For example, in order to measure electrical conductivity, Ohmic contacts have to be formed. Considering a relatively limited published experience of fabricating SiC NW devices or test structures for NW characterization, an important objective of this work was to evaluate a potential and develop as much as possible a convenient NW-device fabrication method. Two different methods were attempted: (1) a conventional photolithography and (2) an FIB deposition.

The photolithography technique was found to be difficult to implement in practice for the available lengths of the NWs investigated in this dissertation. FIB provides an attractive alternative to conventional photolithography by allowing direct metal contact deposition at much smaller scales compared to what is possible with the photolithography. Very small contacts (submicron dimensions) and contact spacings are possible even with randomly oriented NWs.

A basic I-V characteristic, extraction of the "effective" NW conductivity and rough evaluation of the NW doping has been conducted. More reliable measurements eliminating contribution of contact resistance and other factors were not possible in this work because of the electric current induced failure of the FIB fabricated contacts. The failure seems unavoidable even for the moderate values of the current density and possibly reflects an insufficient quality of the Pt electrodes deposited by FIB. The

limitations of the FIB-based process for NW test-structure fabrication have been evaluated to come up with recommendation for the future work.

There is an interesting possibility of utilizing the preferential orientations of the NWs grown on SiC substrates for test-structure or device fabrication instead of harvesting the NWs transferring them to a new substrate. This possibility has not been explored in this work and remains the subject of future research.

REFERENCES

[1] N. Taniguchi, “On the Basic Concept of ‘Nano-Technology’,” *Bulletin of the Japan Society of Precision Engineering*, pp. 18–23, 1974.

[2] R. P. Feynman, “There’s plenty of room at the bottom,” *Journal of Microelectromechanical Systems*, vol. 1, no. 1, pp. 60–66, Mar. 1992.

[3] W. Lu and C. M. Lieber, “Semiconductor nanowires,” *Journal of Physics D: Applied Physics*, vol. 39, no. 21, pp. R387–R406, Nov. 2006.

[4] F. Zhao, H. Chen, S. Deng, and N. Xu, “Ultrafast blue light emission from SiC nanowires,” *Chinese Optics Letters*, vol. 5, no. 3, pp. 184–186, 2007.

[5] M. Kuno, *Introductory Nanoscience: Physical and Chemical Concepts*, 1st ed. Garland Science, 2011, p. 230.

[6] K. K. Nanda, A. Maisels, F. E. Kruis, H. Fissan, and S. Stappert, “Higher Surface Energy of Free Nanoparticles,” *Physical Review Letters*, vol. 91, no. 10, p. 106102, Sep. 2003.

[7] R. Wu, B. Li, M. Gao, J. Chen, Q. Zhu, and Y. Pan, “Tuning the morphologies of SiC nanowires via the control of growth temperature, and their photoluminescence properties.,” *Nanotechnology*, vol. 19, no. 33, p. 335602, Aug. 2008.

[8] A. Agarwal, K. Buddharaju, I. K. Lao, N. Singh, N. Balasubramanian, and D. L. Kwong, “Silicon nanowire sensor array using top–down CMOS technology,” *Sensors and Actuators A: Physical*, vol. 145–146, pp. 207–213, Jul. 2008.

[9] S.-J. Chang, T.-J. Hsueh, C.-L. Hsu, Y.-R. Lin, I.-C. Chen, and B.-R. Huang, “A ZnO nanowire vacuum pressure sensor.,” *Nanotechnology*, vol. 19, no. 9, p. 095505, Mar. 2008.

[10] D. R. Kim, C. H. Lee, and X. Zheng, “Probing flow velocity with silicon nanowire sensors.,” *Nano letters*, vol. 9, no. 5, pp. 1984–8, May 2009.

[11] G. E. Moore, “Cramming More Components Onto Integrated Circuits,” *Proceedings of the IEEE*, vol. 86, no. 1, pp. 82–85, Jan. 1998.

[12] P. Apte, B. Doering, and P. Gargini, “2010 Update Overview,” *INTERNATIONAL TECHNOLOGY ROADMAP FOR SEMICONDUCTORS*, 2010. [Online]. Available: http://www.itrs.net/Links/2010ITRS/Home2010.htm. [Accessed: 25-May-2013].

[13] R. Chau, M. Doczy, B. Doyle, S. Datta, G. Dewey, J. Kavalieros, B. Jin, M. Metz, A. Majumdar, and M. RadosavIjevic, “Advanced CMOS transistors in the nanotechnology era for high-performance, low-power logic applications,” in *Proceedings. 7th International Conference on Solid-State and Integrated Circuits Technology, 2004.*, 2004, vol. 1, pp. 26–30.

[14] J. Xiang, W. Lu, Y. Hu, Y. Wu, H. Yan, and C. M. Lieber, “Ge/Si nanowire heterostructures as high-performance field-effect transistors.,” *Nature*, vol. 441, no. 7092, pp. 489–93, May 2006.

[15] A. Fujiwara, H. Inokawa, K. Yamazaki, H. Namatsu, Y. Takahashi, N. M. Zimmerman, and S. B. Martin, “Single electron tunneling transistor with tunable barriers using silicon nanowire metal-oxide-semiconductor field-effect transistor,” *Applied Physics Letters*, vol. 88, no. 5, p. 053121, 2006.

[16] Z. Fan and J. G. Lu, “Chemical sensing with ZnO nanowire,” in *5th IEEE Conference on Nanotechnology, 2005.*, 2005, pp. 557–560.

[17] F. Patolsky, G. Zheng, and C. M. Lieber, “Nanowire sensors for medicine and the life sciences,” *Nanomedicine*, vol. 1, no. 1, p. 15, 2006.

[18] Y. Dan, Y. Cao, T. E. Mallouk, S. Evoy, and a T. C. Johnson, “Gas sensing properties of single conducting polymer nanowires and the effect of temperature.,” *Nanotechnology*, vol. 20, no. 43, p. 434014, Oct. 2009.

[19] Y. Li, F. Qian, J. Xiang, and C. M. Lieber, “Nanowire electronic and optoelectronic devices,” *Materials Today*, vol. 9, no. 10, pp. 18–27, Oct. 2006.

[20] J. Casady and R. Johnson, “Status of silicon carbide (SiC) as a wide-bandgap semiconductor for high-temperature applications: A review,” *Solid-State Electronics*, vol. 39, no. 10, pp. 1409–1422, Oct. 1996.

[21] M. Treu, R. Rupp, P. Blaschitz, and J. Hilsenbeck, “Commercial SiC device processing: Status and requirements with respect to SiC based power devices,” *Superlattices and Microstructures*, vol. 40, no. 4–6, pp. 380–387, Oct. 2006.

[22] M. Bhatnagar and B. J. Baliga, “Comparison of 6H-SiC, 3C-SiC, and Si for power devices,” *IEEE Transactions on Electron Devices*, vol. 40, no. 3, pp. 645–655, Mar. 1993.

[23] A. M. Ivanov, N. B. Strokan, D. V Davydov, N. S. Savkina, A. A. Lebedev, Y. T. Mironov, G. A. Ryabov, and E. M. Ivanov, "Radiation hardness of SiC ion detectors under relativistic protons," *Semiconductors*, vol. 35, no. 4, pp. 481–484, 2001.

[24] W. Lu, P. Xie, and C. M. Lieber, "Nanowire Transistor Performance Limits and Applications," *IEEE Transactions on Electron Devices*, vol. 55, no. 11, pp. 2859–2876, Nov. 2008.

[25] K. Young, "Short-channel effect in fully depleted SOI MOSFETs," *IEEE TRANSACTIONS ON ELECTRON DEVICES*, vol. 36, no. 2, pp. 2–5, 1989.

[26] R. Yan, A. Ourmazd, and K. Lee, "Scaling the Si MOSFET: From bulk to SOI to bulk," *IEEE TRANSACTIONS ON ELECTRON DEVICES*, vol. 39, no. 7, pp. 704–710, 1992.

[27] K. Zekentes and K. Rogdakis, "SiC nanowires: material and devices," *Journal of Physics D: Applied Physics*, vol. 44, no. 13, p. 133001, Apr. 2011.

[28] W. M. Zhou, F. Fang, Z. Y. Hou, L. J. Yan, and Y. F. Zhang, "Field-effect transistor based on /spl beta/-SiC nanowire," *IEEE Electron Device Letters*, vol. 27, no. 6, pp. 463–465, Jun. 2006.

[29] C.-O. Jang, T.-H. Kim, S.-Y. Lee, D.-J. Kim, and S.-K. Lee, "Low-resistance ohmic contacts to SiC nanowires and their applications to field-effect transistors.," *Nanotechnology*, vol. 19, no. 34, p. 345203, Aug. 2008.

[30] H. Seong, H.-J. Choi, S.-K. Lee, J. Lee, and D. Choi, "Optical and electrical transport properties in silicon carbide nanowires," *Applied Physics Letters*, vol. 85, no. 7, p. 1256, 2004.

[31] Y. Chen, X. Zhang, Q. Zhao, L. He, C. Huang, and Z. Xie, "P-type 3C-SiC nanowires and their optical and electrical transport properties.," *Chemical communications (Cambridge, England)*, vol. 47, no. 22, pp. 6398–400, Jun. 2011.

[32] B. Krishnan, R. V. K. G. Thirumalai, Y. Koshka, S. Sundaresan, I. Levin, A. V Davydov, and J. N. Merrett, "Substrate-Dependent Orientation and Polytype Control in SiC Nanowires Grown on 4H-SiC Substrates," *Crystal Growth & Design*, vol. 11, no. 2, pp. 538–541, Feb. 2011.

[33] X. Li, X. Wang, R. Bondokov, J. Morris, Y. H. An, and T. S. Sudarshan, "Micro/nanoscale mechanical and tribological characterization of SiC for orthopedic applications.," *Journal of biomedical materials research. Part B, Applied biomaterials*, vol. 72, no. 2, pp. 353–61, Feb. 2005.

[34] S. Santavirta, M. Takagi, L. Nordsletten, A. Anttila, R. Lappalainen, and Y. T. Konttinen, “Biocompatibility of silicon carbide in colony formation test in vitro,” *Archives of Orthopaedic and Trauma Surgery*, vol. 118, no. 1–2, pp. 89–91, Nov. 1998.

[35] S. E. Saddow, C. Coletti, C. Frewin, N. C. Schettini, A. Oliveros, and M. Jaroszeski, “Single-crystal Silicon Carbide: A Biocompatible and Hemocompatible Semiconductor for Advanced Biomedical Applications,” *MRS Proceedings*, vol. 1246, pp. 824–830, Feb. 2011.

[36] G. Gabriel, I. Erill, J. Caro, R. Gómez, D. Riera, R. Villa, and P. Godignon, “Manufacturing and full characterization of silicon carbide-based multi-sensor micro-probes for biomedical applications,” *Microelectronics Journal*, vol. 38, no. 3, pp. 406–415, Mar. 2007.

[37] H. Y. Wang, Y. Q. Wang, Q. F. Hu, and X. J. Li, “Capacitive humidity sensing properties of SiC nanowires grown on silicon nanoporous pillar array,” *Sensors and Actuators B: Chemical*, vol. 166–167, pp. 451–456, May 2012.

[38] K. Jain, C. G. Willson, and B. J. Lin, “Ultrafast deep UV Lithography with excimer lasers,” *IEEE Electron Device Letters*, vol. 3, no. 3, pp. 53–55, Mar. 1982.

[39] S. F. A. Rahman, U. Hashim, M. N. M. Nor, and M. E. A. Shohini, “Fabrication of nano and micrometer structures using electron beam and optical mixed lithography process,” *Int. J. Nanoelectronics and Materials*, vol. 4, pp. 49–58, 2011.

[40] J. H. Choi, L. Latu-Romain, E. Bano, F. Dhalluin, T. Chevolleau, and T. Baron, “Fabrication of SiC nanopillars by inductively coupled SF 6 /O 2 plasma etching,” *Journal of Physics D: Applied Physics*, vol. 45, no. 23, p. 235204, Jun. 2012.

[41] D. Zhou and S. Seraphin, “Production of silicon carbide whiskers from carbon nanoclusters,” *Chemical Physics Letters*, vol. 222, no. 3, pp. 233–238, May 1994.

[42] W. Zhou, Y. Zhang, X. Niu, and G. Min, *One-Dimensional Nanostructures*. New York, NY: Springer New York, 2008, pp. 17–59.

[43] H. Dai, E. W. Wong, Y. Z. Lu, S. Fan, and C. M. Lieber, “Synthesis and characterization of carbide nanorods,” *Nature*, vol. 375, no. 6534, pp. 769–772, Jun. 1995.

[44] W. Han, S. Fan, Q. Li, W. Liang, B. Gu, and D. Yu, “Continuous synthesis and characterization of silicon carbide nanorods,” *Chemical physics letters*, vol. 4, no. February, pp. 0–4, 1997.

[45] T. Seeger, P. Kohler-Redlich, and M. Rühle, “Synthesis of Nanometer-Sized SiC Whiskers in the Arc-Discharge,” *Advanced Materials*, vol. 12, no. 4, pp. 279–282, Feb. 2000.

[46] A. Thess, R. Lee, P. Nikolaev, H. Dai, P. Petit, J. Robert, C. Xu, Y. Lee, S. Kim, A. Rinzler, D. Colbert, G. Scuseria, D. Tomanek, J. Fischer, and R. Smalley, “Crystalline Ropes of Metallic Carbon Nanotubes,” *Science (New York, N.Y.)*, vol. 273, no. 5274, pp. 483–7, Jul. 1996.

[47] J. Liu, A. Rinzler, H. Dai, J. Hafner, R. Bradley, P. Boul, a Lu, T. Iverson, K. Shelimov, C. Huffman, F. Rodriguez-Macias, Y. Shon, T. Lee, D. Colbert, and R. Smalley, “Fullerene pipes,” *Science (New York, N.Y.)*, vol. 280, no. 5367, pp. 1253–6, May 1998.

[48] W. Shi, Y. Zheng, H. Peng, N. Wang, C. S. Lee, and S.-T. Lee, “Laser Ablation Synthesis and Optical Characterization of Silicon Carbide Nanowires,” *Journal of the American Ceramic Society*, vol. 83, no. 12, pp. 3228–3230, Dec. 2000.

[49] W. M. Zhou, B. Yang, Z. X. Yang, F. Zhu, L. J. Yan, and Y. F. Zhang, “Large-scale synthesis and characterization of SiC nanowires by high-frequency induction heating,” *Applied Surface Science*, vol. 252, no. 14, pp. 5143–5148, May 2006.

[50] W. Yang, H. Araki, S. Thaveethavorn, H. Suzuki, and T. Noda, “In situ synthesis and characterization of pure SiC nanowires on silicon wafer,” *Applied Surface Science*, vol. 241, no. 1–2, pp. 236–240, Feb. 2005.

[51] W. Yang, H. Araki, Q. Hu, N. Ishikawa, H. Suzuki, and T. Noda, “In situ growth of SiC nanowires on RS-SiC substrate(s),” *Journal of Crystal Growth*, vol. 264, no. 1–3, pp. 278–283, Mar. 2004.

[52] Y. Ying, Y. Gu, Z. Li, H. Gu, L. Cheng, and Y. Qian, “A simple route to nanocrystalline silicon carbide,” *Journal of Solid State Chemistry*, vol. 177, no. 11, pp. 4163–4166, Nov. 2004.

[53] R. S. Wagner and W. C. Ellis, “Vapor-Liquid-Solid Mechanism of Single Crystal Growth,” *Applied Physics Letters*, vol. 4, no. 5, p. 89, 1964.

[54] H. Choi, “Vapor–Liquid–Solid Growth of Semiconductor Nanowires,” in *Semiconductor Nanostructures for Optoelectronic Devices Processing, Characterization and Applications*, G.-C. Yi, Ed. Berlin, Heidelberg: Springer Berlin Heidelberg, 2012, pp. 1–36.

[55] A. S. Edelstein, D. J. Gillespie, S. F. Cheng, J. H. Perepezko, and K. Landry, “Reactions at amorphous SiC/Ni interfaces,” *Journal of Applied Physics*, vol. 85, no. 5, p. 2636, 1999.

[56] R. C. J. Schiepers, J. a. van Beek, F. J. J. van Loo, and G. de With, "The interaction between SiC and Ni, Fe, (Fe,Ni) and steel: Morphology and kinetics," *Journal of the European Ceramic Society*, vol. 11, no. 3, pp. 211–218, Jan. 1993.

[57] M. H. Huang, Y. Wu, H. Feick, N. Tran, E. Weber, and P. Yang, "Catalytic Growth of Zinc Oxide Nanowires by Vapor Transport," *Advanced Materials*, vol. 13, no. 2, pp. 113–116, Jan. 2001.

[58] B. A. Wacaser, K. A. Dick, J. Johansson, M. T. Borgström, K. Deppert, and L. Samuelson, "Preferential Interface Nucleation: An Expansion of the VLS Growth Mechanism for Nanowires," *Advanced Materials*, vol. 21, no. 2, pp. 153–165, Jan. 2009.

[59] H. Young Kim, J. Park, and H. Yang, "Direct synthesis of aligned silicon carbide nanowires from the silicon substrates," *Chemical Communications*, vol. 0, no. 2, pp. 256–257, 2003.

[60] H. Wang, Z. Xie, W. Yang, J. Fang, and L. An, "Morphology Control in the Vapor-Liquid-Solid Growth of SiC Nanowires," *Crystal Growth & Design*, vol. 8, no. 11, pp. 3893–3896, 2008.

[61] F. Gao, W. Yang, H. Wang, Y. Fan, Z. Xie, and L. An, "Controlled Al-Doped Single-Crystalline 6H-SiC Nanowires," *Crystal Growth & Design*, vol. 8, no. 5, pp. 1461–1464, 2008.

[62] Z. Pan, H.-L. Lai, F. C. K. Au, X. Duan, W. Zhou, W. Shi, N. Wang, C.-S. Lee, N.-B. Wong, S.-T. Lee, and S. Xie, "Oriented Silicon Carbide Nanowires: Synthesis and Field Emission Properties," *Advanced Materials*, vol. 12, no. 16, pp. 1186–1190, Aug. 2000.

[63] S. G. Sundaresan, A. V Davydov, M. D. Vaudin, and I. Levin, "Growth of Silicon Carbide Nanowires by a Microwave Heating-Assisted Physical Vapor Transport Process Using Group VIII Metal Catalysts," *Chem. Mater.*, vol. 19, no. 23, pp. 5531–5537, 2007.

[64] R. Pampuch, G. Gorny, and L. Stobierski, "Synthesis of One-Dimensional Nanostructured Silicon Carbide by Chemical Vapor Deposition 1," *Glass Phys. Chem.*, vol. 31, no. 3, pp. 370–376, 2005.

[65] H.-K. Seong, T.-E. Park, S.-C. Lee, K.-R. Lee, J. Park, and H. Choi, "Magnetic properties of vanadium-doped silicon carbide nanowires," *Metals and Materials International*, vol. 15, no. 1, pp. 107–111, Feb. 2009.

[66] M. Bechelany, A. Brioude, D. Cornu, G. Ferro, and P. Miele, "A Raman Spectroscopy Study of Individual SiC Nanowires," *Advanced Functional Materials*, vol. 17, no. 6, pp. 939–943, Apr. 2007.

[67] H. Wang, L. Lin, W. Yang, Z. Xie, and L. An, “Preferred Orientation of SiC Nanowires Induced by Substrates,” *J. Phys. Chem. C*, vol. 114, no. 6, pp. 2591–2594, 2010.

[68] H. Y. Peng, X. T. Zhou, H. L. Lai, N. Wang, and S. T. Lee, “Microstructure observations of silicon carbide nanorods,” *J. Mater. Res.*, vol. 15, no. 9, pp. 2020–2026, 2000.

[69] Y. Yao, S. T. Lee, and F. H. Li, “Direct synthesis of 2H–SiC nanowhiskers,” *Chemical Physics Letters*, vol. 381, no. 5–6, pp. 628–633, Nov. 2003.

[70] S. Kotamraju, B. Krishnan, Y. Koshka, S. Sundaresan, H. Issa, and R. Singh, “Silicon carbide nanowires grown on 4H-SiC substrates by chemical vapor deposition,” *MRS Proceedings*, vol. 1178, pp. 1178–AA03–06, Jan. 2011.

[71] H. Yoshida, H. Kohno, S. Ichikawa, T. Akita, and S. Takeda, “Inner potential fluctuation in SiC nanowires with modulated interior structure,” *Materials Letters*, vol. 61, no. 14–15, pp. 3134–3137, Jun. 2007.

[72] B. Krishnan, S. P. Kotamraju, S. G. Sundaresan, and Y. Koshka, “SiC Nanowires Grown on 4H-SiC Substrates by Chemical Vapor Deposition,” *Materials Science Forum*, vol. 645–648, pp. 187–190, Apr. 2010.

[73] J. M. Zuo and J. C. Mabon, “Web-Based Electron Microscopy Application Software: Web-EMAPS,” *Microscopy and Microanalysis*, vol. 10, no. S02, pp. 1000–1001, Aug. 2004.

[74] R. V. K. G. Thirumalai, B. Krishnan, A. V. Davydov, J. N. Merrett, and Y. Koshka, “SiC nanowire vapor–liquid–solid growth using vapor-phase catalyst delivery,” *Journal of Materials Research*, vol. FirstView, pp. 1–7, Jul. 2012.

[75] S. Kotamraju, B. Krishnan, G. Melnychuk, and Y. Koshka, “Low-temperature homoepitaxial growth of 4H–SiC with CH3Cl and SiCl4 precursors,” *Journal of Crystal Growth*, vol. 312, no. 5, pp. 645–650, Feb. 2010.

[76] F. La Via, F. Roccaforte, V. Raineri, M. Mauceri, A. Ruggiero, P. Musumeci, L. Calcagno, A. Castaldini, and A. Cavallini, “Schottky–ohmic transition in nickel silicide/SiC-4H system: is it really a solved problem?,” *Microelectronic Engineering*, vol. 70, no. 2–4, pp. 519–523, Nov. 2003.

[77] B. Krishnan, S. P. Kotamraju, G. Melnychuk, H. Das, J. N. Merrett, and Y. Koshka, “Heavily Aluminum-Doped Epitaxial Layers for Ohmic Contact Formation to p-Type 4H-SiC Produced by Low-Temperature Homoepitaxial Growth,” *Journal of Electronic Materials*, vol. 39, no. 1, pp. 34–38, 2010.